NOVEL HYBRID LIGHT EMITTING DIODES WITH MULTIPLE ASSEMBLIES OF NANOCRYSTALS TO GENERATE AND TUNE WHITE LIGHT

A THESIS
SUBMITTED TO THE DEPARTMENT OF PHYSICS
AND THE INSTITUTE OF ENGINEERING AND SCIENCES
OF BILKENT UNIVERSITY
IN PARTIAL FULLFILMENT OF THE REQUIREMENTS
FOR THE DEGREE OF
MASTER OF SCIENCE

By
Sedat Nizamoğlu
June 2007

I certify that I have read this thesis and that in my opinion it is fully adequate, in scope and in quality, as a thesis for the degree of Master of Science.

Assist. Prof. Dr. Hilmi Volkan Demir (Supervisor)

I certify that I have read this thesis and that in my opinion it is fully adequate, in scope and in quality, as a thesis for the degree of Master of Science.

Assist. Prof. Dr. Mehmet Özgür Oktel

I certify that I have read this thesis and that in my opinion it is fully adequate, in scope and in quality, as a thesis for the degree of Master of Science.

Assist. Prof. Dr. Dönüş Tuncel

Approved for the Institute of Engineering and Sciences:

Prof. Dr. Mehmet B. Baray
Director of Institute of Engineering and Sciences

ABSTRACT

NOVEL HYBRID LIGHT EMITTING DIODES WITH MULTIPLE ASSEMBLIES OF NANOCRYSTALS TO GENERATE AND TUNE WHITE LIGHT

Sedat Nizamoğlu
M.S. in Physics
Supervisor: Assist. Prof. Dr. Hilmi Volkan Demir

June 2007

Today approximately one third of the world population (about two billion people) in under-developed countries has no access to electricity and relies on unhealthy, costly and low-quality fuel-based lighting for home illumination. In the rest of the world, lighting consumes a large portion (20%) of the total electricity production, which significantly contributes to global warming problem. Also given limited resources, such large energy consumption needs to be reduced for sustainable economic growth. Solid state lighting provides remedy to these problems for the entire globe. Therefore, the advancement of white light emitting diodes (WLEDs) becomes a key point for development of human civilization. To this end, the strong demand for the development of high quality WLEDs around the globe motivates our research work on the investigation of white light generation with high color rendering index.

In this thesis, we develop and demonstrate nanocrystal hybridized light emitting diodes with high color rendering index. By the hybridization of multiple layer-by-layer assemblies of CdSe/ZnS core-shell nanocrystals on blue and near ultraviolet (n-UV) InGaN/GaN light emitting diodes, we show white

light generation with highly tunable optical properties such as tristimulus color coordinates, correlated color temperature, and color rendering index. Additionally, by using dual hybridization of nanocrystals in combination with conjugated polymers, we obtain white light sources with high color rendering indices exceeding the requirements of the future solid state lighting applications. In this thesis, we present design, growth, fabrication, experimental characterization and theoretical analysis of these hybrid white LEDs.

Keywords: white light, light emitting diode, color rendering index, tunable, nanocrystal, hybridization, InGaN/GaN, blue, near ultraviolet.

ÖZET

BEYAZ IŞIĞIN AYARLANMASI VE ÜRETİLMESİ İÇİN YENİ MELEZ NANOKRİSTAL TABANLI IŞIK YAYAN DİYOTLAR

Sedat Nizamoğlu
Fizik Bölümü Yüksek Lisans
Tez Yöneticisi: Yrd. Doç. Dr. Hilmi Volkan Demir
Haziran 2007

Günümüzde yaklaşık dünya nüfusunun üçte biri (iki milyar insan) az gelişmiş ülkelerde elektriğe erişememekte ve sağlıksız, pahalı ve düşük kaliteli sıvı yakıt tabanlı aydınlatma kaynaklarını evlerde kullanmaktadır. Dünyanın geri kalanında ise aydınlatma %20 gibi büyük bir oranda üretilen elektriği tüketmekte ve bu da küresel ısınma problemini daha ciddi hale getirmektedir. Kaynakların sınırlı olmasından dolayı, ekonomik büyümenin sürdürülebilmesi için, mevcut olan yüksek enerji tüketiminin azaltılması gerekmektedir. Katı hal tabanlı aydınlatmalar bu problemlere karşı küresel bir çözüm niteliği taşımaktadır. Bu yüzden, beyaz LED'lerin (ışık yayan diyotların) geliştirilmesi insanlık açısından büyük önem taşımaktadır. Yüksek kaliteli beyaz LED'lerin geliştirilmesi konusundaki küresel beklenti araştırma çalışmalarımızdaki motivasyon kaynağımızı oluşturmaktadır.

Bu tez çalışmasında, nanokristal tabanlı yüksek renk dönüşüm indeksine sahip LED'leri çalıştık. CdSe/ZnS çekirdek-kabuk nanokristallerin mavi ve yakın morötesi dalgaboylarındaki LED'ler ile çok katmanlı olarak melezleştirilmesi sonucunda, renk kordinatı, renk sıcaklığı ve renk dönüşüm indeksi gibi optik parametrelerin yüksek ayarlanabilirliliğini gösterdik. Ek olarak, gelecekte beyaz LED'lerin ulaşması öngörülen yüksek renk dönüşüm indeksini, nanokrsital ve konjuge polimerlerle beraber kullanarak elde ettik. Bu tezde, melez beyaz LED'lerimizin tasarımı, büyütmesi, fabrikasyonu, deneysel karakterizasyonu ve kuramsal analizlerini gerçekleştirdik.

Anahtar kelimeler: beyaz ışık, LED, renk dönüşüm indeksi, ayarlanabilir, nanokristal, melezleştirme, InGaN/GaN, mavi, yakın morötesi.

Acknowledgements

It is for me a great honor and pleasure being Prof. Hilmi Volkan Demir's graduate student. His kind, positive, friendly and warm personality and management embraced us, and his invaluable guidance, motivation, encouragement, confidence, understanding, and endless support made him more than a supervisor for me. I learnt a lot from him about academic and social life.

Almost in each experimental setup, I can feel Prof. Ekmel Özbay's great contribution to national science and makes him another great example for me. Each day, I feel the progress in our research facilities with the great contribution both by Prof. Özbay and Prof. Demir. Additionally Prof. Özbay's research group helped me a lot about the experimental setups and measurements.

I would like to thank Prof. Mehmet Özgür Oktel for his great contribution to my understanding in quantum mechanics and in the quantum mechanical calculation in this thesis. His positive and warm personality made the quantum mechanics courses and calculations very enjoyable.

I want to thank to all my friends in our Demir Sensor and Devices Research Group: Evren Mutlugün, Emre Sarı, Tuncay Özel, İbrahim Murat Soğancı, Rohat Melik, İlkem Özge Hüyal, Can Uran, Sümeyra Tek, Güliz Zengin, Özgün Akyüz, Emre Ünal, Aslı Koç, additionally, Atilla Özgür Çakmak from Özbay group. My home mate Evren Mutlugün is really a great person, we had very funny days in research, courses and friendship and he remembered me different aspects of life. Yılmaz Dikme significantly contributed us in MOCVD growths.

Also, Yeşim Balıkçıoğlu helped us a lot in organization of our international conferences. Ahmet Levent Subaşı's great advices and discussions about courses made my life easier. During my MS courses in Bilkent Physics, I meet with many famous physicists in their areas from who I learnt a lot. Additionally, I want to thank to professors and researchers in Nanotechnology Research Center and Advanced Research Laboratory as well. Aşkın Kocabaş and Münir Dede also significantly helped me in clean room work. I want to thank all staff in Bilkent who provide a peaceful place for us for research.

I want to thank to our research colleges Dönüş Tuncel in Chemistery Department; Sameer Sapra, Nikolai Gaponik, Alexandre Eychmüller in Technical University of Dresden and Elisabeth Holder and Nan Tian in University of Wuppertal. Without the help and support of great people mentioned in this text, this research work would not have been able to go this far.

Finally, I want to thank to my lovely family: my father Alican, my mother Aynur and my sister İrem. Also my friends who gave me the life happiness…

Table of Contents

List of Figures

List of Tables

Chapter 1

Introduction

Recently solid-state lighting using white light emitting diodes (WLEDs) has attracted world-wide attention because of the important economical and technological benefits for people in under-developed, developing and developed countries in terms of energy-saving, safety, reliability, maintenance, and high color quality [1]. Today two billion people around the world live in under-developed countries without electricity [2]. They use fuel based lighting for home illumination that causes an unhealthy and costly means of illumination with low light quality (e.g., low color rendering index) and people who cannot afford this kind of lighting cannot perform critical modern day evening activities such as reading, working and trading. Therefore, the advancement of solid state lighting with renewable energy sources is a key to the human development (e.g., the improvement of literacy and education) for the under-developed part of the world. For the two third of world population that live in developing and developed countries using electricity, it is estimated that 20% of the electricity production is currently consumed for lighting and solid-state lighting offers potentially 50% reduction globally in the electricity consumption for illumination [3]. Therefore, given the limited remaining resources and the current growth rates of countries, solid-state white light emitting devices are

critical for new industry and job areas and sustainable economic growth. Furthermore, regarding the global warming issue, solid state lighting provides an important solution to decrease the CO_2 reduction about 300 million metric tons annually as well [2]. To this end, the world-wide strong demand for the development of high quality WLEDs around the globe motivates our research work on the investigation of white light generation with high color rendering index in this thesis. For that, we develop and demonstrate nanocrystal hybridized tunable light emitting diodes with high color rendering index. In this thesis, we present design, epitaxial growth, fabrication, experimental and theoretical analysis of these hybrid white LEDs.

This thesis is organized as follows: In Chapter 1, we present a general introduction to the solid state lighting. In Chapter 2, we continue with the general concepts and parameters about light sources. In Chapter 3, we explain different methods for white light emitting diodes. In Chapter 4, we look at the synthesis, characterization and theoretical analysis of nanocrystals. In Chapter 5, we present nanocrystal based hybrid LEDs to generate and tune white light. In Chapter 6, we close our thesis with our conclusions.

Incandescent lamps: They are called electric lamps, arc lamp, light globes in Australia and more commonly light bulbs in Anglophone countries [4]. An electrical current passes through a thin filament. Because of the resistance of filament, the filament gets hotter, becomes excited and as a result thermally equilibrated photons are released. The efficiency of this process is very low

because only 2% of the its energy can be used as visible light, the rest is wasted by heat and infrared light.

Fluorescent lamps: The electric current passes mercury vapor that produces ultraviolet light [4]. The ultraviolet light is then absorbed by phosphorus coating that is inside the lamp. Afterward the phosphorus makes photoluminescence in visible spectrum. In fluorescent lamps the heat leakage is much less than incandescent lamps. However, efficiencies decrease because of ultraviolet light generation and convert ion of this light into visible light.

Solid State Lighting: Solid-state lighting (SSL) uses semiconductor materials converting electric energy into light. The electric current passes through the diode in forward bias mode. As the electrons and holes pass through the diode, they recombine and photons are generated. (More detailed information will be given in Chapter 3.)

In Table 1.1, we show the general comparison of current technologies [5,6].

	Advantages	**Disadvantages**
Incandascent lamps	+ Dimmable + High color quality + Low lamp cost	+ High wattage + Short life + Heat increases cooling load
Flourescent lamps	+ High efficacy + Long life	+ Few dimmable products + More expensive than

		incandascent lamps. + Replacement lamps can be difficult to find (depending on the type of flourescent lamps)
Solid State LEDs	+ High efficacy + long life time + design flexibility + directional light + robustness + dimming capability without color shift + absence of heat or UV in light beam + low-voltage d.c. operation	+ Relatively low light output + Expensive + Sensitive to high-temperature environment + Replacement lamps not available

Table 1.1. General comparison of current technologies.

In Table 1.2, we make a technical comparison of current and future technologies [7].

	Future solid state lighting	Today solid state lighting	Incandascent	Flourescent
Luminous efficacy (lm/W)	200	50-70	16	85
Lifetime (kh)	>100	20	1	10
Flux (lm/lamp)	1,500	200	1,200	3,400
Input power (W/lamp)	7.5	1.2-2.6	75	20
Lumen cost ($/klm)	< 2	20	0.4	1.5
Lamp cost ($/lamp)	<3	4	0.5	5
Color Rendering Index (CRI)	>80	70-80	95	75

Table 1.2. Technical comparison of current and future technologies.

Chapter 2

General concepts and parameters about light sources

2.1. Technical concepts

Radiometric units: The physical properties of electromagnetic radiation are characterized by radiometric units in terms of number of photons, photon energy and optical power (also called radiant flux) [8].

Photometric units: Photometric units characterize the light and color sensation by the human eye. The following concepts are photometric units.

Eye sensitivity function: The function that converts radiometric units to photometric units. The mostly commonly referred eye sensitivity function is CIE 1931 V(λ) function that is the current photometric standard in the United States.

Luminous intensity: Luminous intensity shows the light intensity of an optical source that is received by human eye. It is measured in units of candela (cd), which is an unit of the International System of Units (SI units).

Another current definition of luminous intensity is as follows: a monochromatic light source emitting an optical power of (1/683) watt at 555 nm into the solid angle of 1 steradian (sr) has a luminous intensity of 1 candela (cd).

Luminous flux: Luminous flux shows the light power of an optical source that is received by the human eye. Its unit is lumen (lm).

$$\Phi_{lum} = 683 \text{ lm/W} \int_{\lambda} V(\lambda)P(\lambda)d\lambda, \quad (2.1.1)$$

where $P(\lambda)$ is the power spectral density.

Illuminance: Illuminance is the luminous flux incident per unit area. Its unit is lux which is lm/m^2. For example, the illuminance of full moon is 1 lux and the illuminance of direct sunlight is 100000 lux.

Luminance: The ratio of the luminous intensity emitted in a certain direction divided by the projected surface area in that direction. Its unit is cd/m^2.

Luminous efficacy: Luminous efficacy is the conversion efficiency from optical power to luminous flux.

$$\text{Luminous efficacy} = \Phi_{lum}/P = [683 \text{ lm/W} \int_{\lambda} V(\lambda)P(\lambda)d\lambda] / [\int_{\lambda} P(\lambda)d\lambda] \quad (2.1.2)$$

Luminous efficiency: Luminous efficiency is the luminous flux of the light source divided by the electrical input power. For instance, luminous efficiency of fluorescent light tubes are 50-80 lm/W.

$$\text{Luminous efficiency} = \Phi_{lum}/(IV) \quad (2.1.3)$$

2.2 Color-matching function and chromaticity diagram

Since the sensation of color may change from one person to another one, the International Commission for Illimunation (Commission Internationale de l'Eclairage, CIE) standardized measurement of color through color-matching functions and the chromaticity diagram. The color matching functions are obtained by using two lights side by side, one being monochromatic and the

other one being a mixture of three primary lights with color red, green and blue. By adjusting the relative intensities of the red, green and blue lights a person can adjust to match them when the two lights appear identical. Through these matches the three color-matching functions are obtained. The CIE 1931 color matching functions x(λ), y(λ) and z(λ) are shown in Figure 2.2.1. The green color matching function in the Figure 2.2.1 which one is identical to the eye sensitivity function.

$$y(\lambda)=V(\lambda) \tag{2.2.1}$$

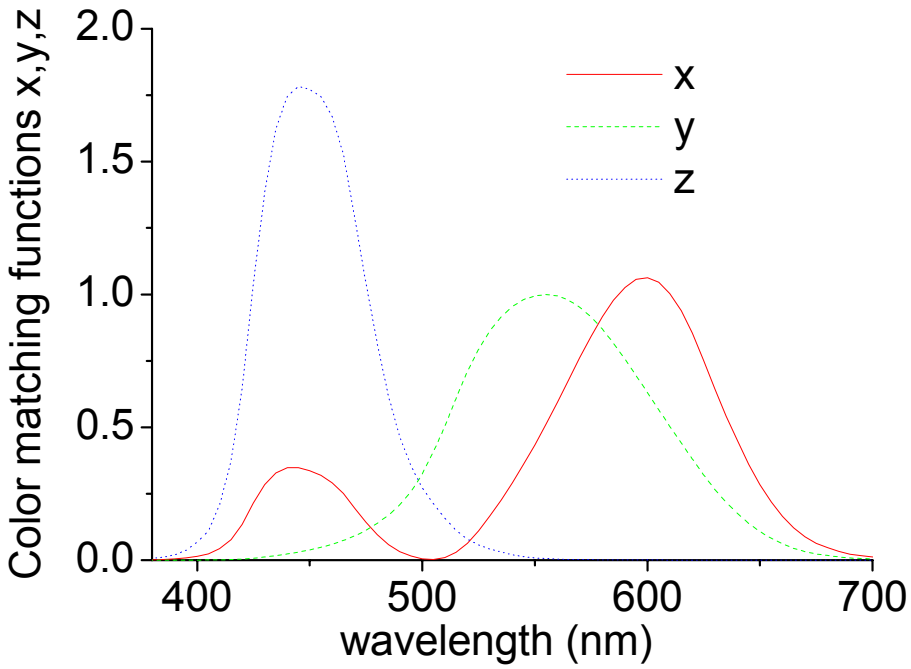

Figure 2.2.1. Spectral distribution of Color matching functions.

For a given power spectral density, the X, Y and Z tristimulus values are calculated as following:

$$X = \int_{\lambda} x(\lambda)P(\lambda)d\lambda \tag{2.2.2}$$

$$Y = \int_{\lambda} y(\lambda)P(\lambda)d\lambda \quad (2.2.3)$$

$$Z = \int_{\lambda} z(\lambda)P(\lambda)d\lambda \quad (2.2.4)$$

Although the units of X,Y and Z values seem Watt, they are unitless because in front of the integral there is a 1/Watt prefactor that makes them unitless. The chromaticity coordinates are calculated by using the tristimulus coordinates as following:

$$x = X/(X+Y+Z) \quad (2.2.5)$$

$$y = Y/(X+Y+Z) \quad (2.2.6)$$

$$z = Z/(X+Y+Z) = 1-x-y \quad (2.2.7)$$

The (x,y) chromaticity diagram is shown in Figure 2.2.2.

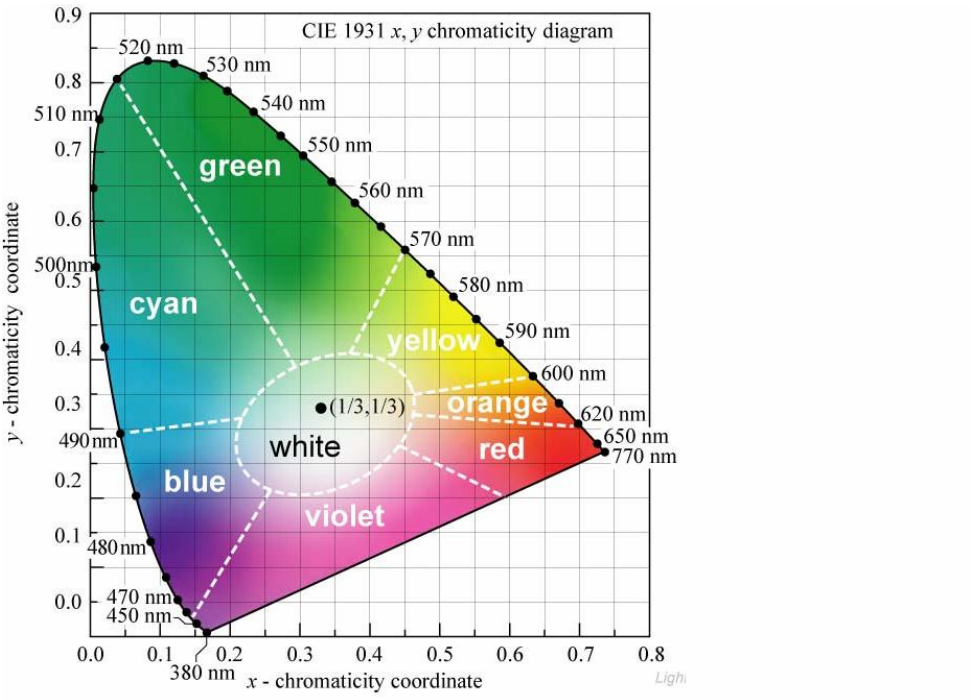

Figure 2.2.2. CIE 1931 (x,y)chromaticity diagram (After Ref. 8).

The equal energy point located in the center of the chromaticity diagram is at (x,y,z) = (1/3,1/3,1/3).

2.3 Color temperature

There exist a large number of optical spectra which white light can be obtained. By using planckian black-body radiation spectrum with its color temperature the white light and other visible spectra can be described. The black-body spectrum depending on wavelength is as following [8]:

$$I(\lambda) = \frac{2hc^2}{\lambda^5[\exp(\frac{hc}{\lambda kT}) - 1]} \tag{2.3.1}$$

As the temperature of the black-body increases, the chromaticity follows the colors red, orange, yellowish white, white, and bluish white. The unit of the color temperature is Kelvin and color temperature shows the chromaticity diagram location on the planckian locus. However, should not the (x,y) coordinate of the white light source fall on the planckian locus, the correlated color temperatue is used whose unit is Kelvin as well. In Figure 2.2.3, Illuminant A is incandescent source with T=2856 K and (x,y)= (0.44, 0.40), Illuminant B is direct sunlight with T=4870 K and (x,y)= (0.34, 0.35) and Illuminant E is equal energy point with (x,y)= (0.33, 0.33).

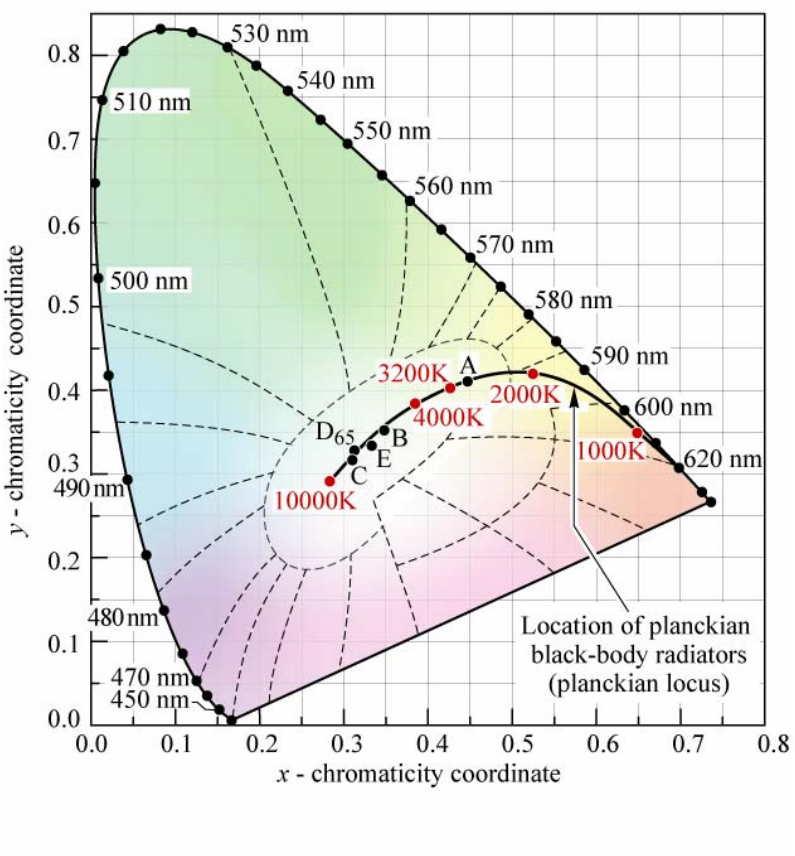

Figure 2.2.3. Chromaticity diagram showing planckian locus. (After Ref. 8)

The correlated color temperature is calculated by looking at the nearest distant plankian locus point on the (u',v') chromaticity diagram to a white light source. The (u',v') point which is a transformation of (x,y) point is calculated as following:

$$u' = \frac{4X}{X + 15Y + 3Z} \tag{2.3.2}$$

$$v' = \frac{9Y}{X + 15Y + 3Z} \tag{2.3.3}$$

Light source	Correlated color temperature (K)
"Warm white" flourescent tube	3000
"Cool daylight white" flourescent tube	4300
Xenon Arc	6000
Direct sun	5700-6500
Clear blue sky	8000-27000

Table 2.3.1. Light sources and their correlated color temperature [After Ref. 8].

2.4 Color mixing

Determination of chromaticity coordinates of the mixture emissions is also possible. Assume that there are three emission peaks at wavelengths λ_1, λ_2 and λ_3 with spectral power densities $P_1(\lambda)$, $P_2(\lambda)$ and $P_3(\lambda)$ and with chromaticity tristimulus coordinates (x_1,y_1), (x_2,y_2) and (x_3,y_3) respectively. Then the combined tristimulus coordinate is found as following:

$$X = \int_{\lambda} \bar{x}(\lambda)P_1(\lambda)d\lambda + \int_{\lambda} \bar{x}(\lambda)P_2(\lambda)d\lambda + \int_{\lambda} \bar{x}(\lambda)P_3(\lambda)d\lambda \approx \bar{x}(\lambda_1)P_1 + \bar{x}(\lambda_2)P_2 + \bar{x}(\lambda_3)P_3 \tag{2.4.1}$$

$$Y = \int_{\lambda} \bar{y}(\lambda)P_1(\lambda)d\lambda + \int_{\lambda} \bar{y}(\lambda)P_2(\lambda)d\lambda + \int_{\lambda} \bar{y}(\lambda)P_3(\lambda)d\lambda \approx \bar{y}(\lambda_1)P_1 + \bar{y}(\lambda_2)P_2 + \bar{y}(\lambda_3)P_3 \tag{2.4.2}$$

$$Z = \int_{\lambda} \bar{z}(\lambda)P_1(\lambda)d\lambda + \int_{\lambda} \bar{z}(\lambda)P_2(\lambda)d\lambda + \int_{\lambda} \bar{z}(\lambda)P_3(\lambda)d\lambda \approx \bar{z}(\lambda_1)P_1 + \bar{z}(\lambda_2)P_2 + \bar{z}(\lambda_3)P_3 \tag{2.4.3}$$

$$L_1 = \bar{x}(\lambda_1)P_1 + \bar{y}(\lambda_1)P_1 + \bar{z}(\lambda_1)P_1 \tag{2.4.4}$$

$$L_2 = \bar{x}(\lambda_2)P_2 + \bar{y}(\lambda_2)P_2 + \bar{z}(\lambda_2)P_2 \tag{2.4.5}$$

$$L_3 = \bar{x}(\lambda_3)P_3 + \bar{y}(\lambda_3)P_3 + \bar{z}(\lambda_3)P_3 \tag{2.4.6}$$

$$x = \frac{x_1L_1 + x_2L_2 + x_3L_3}{L_1 + L_2 + L_3} \tag{2.4.7}$$

$$y = \frac{y_1L_1 + y_2L_2 + y_3L_3}{L_1 + L_2 + L_3} \tag{2.4.8}$$

When we mix two colors L_3=P_3=0, the mixed color will be located on a straight line connecting the chromaticity coordinates of two sources. Any color on the line can be generated by mixing the two sources. In the case of three source such as trichromic LED, we can combine the chromaticity coordinate of the sources by three straight line which makes a triangle. This triangle is called the color gamut and all the colors inside of the gamut can be generated, however, any color outside the gamut cannot be generated.

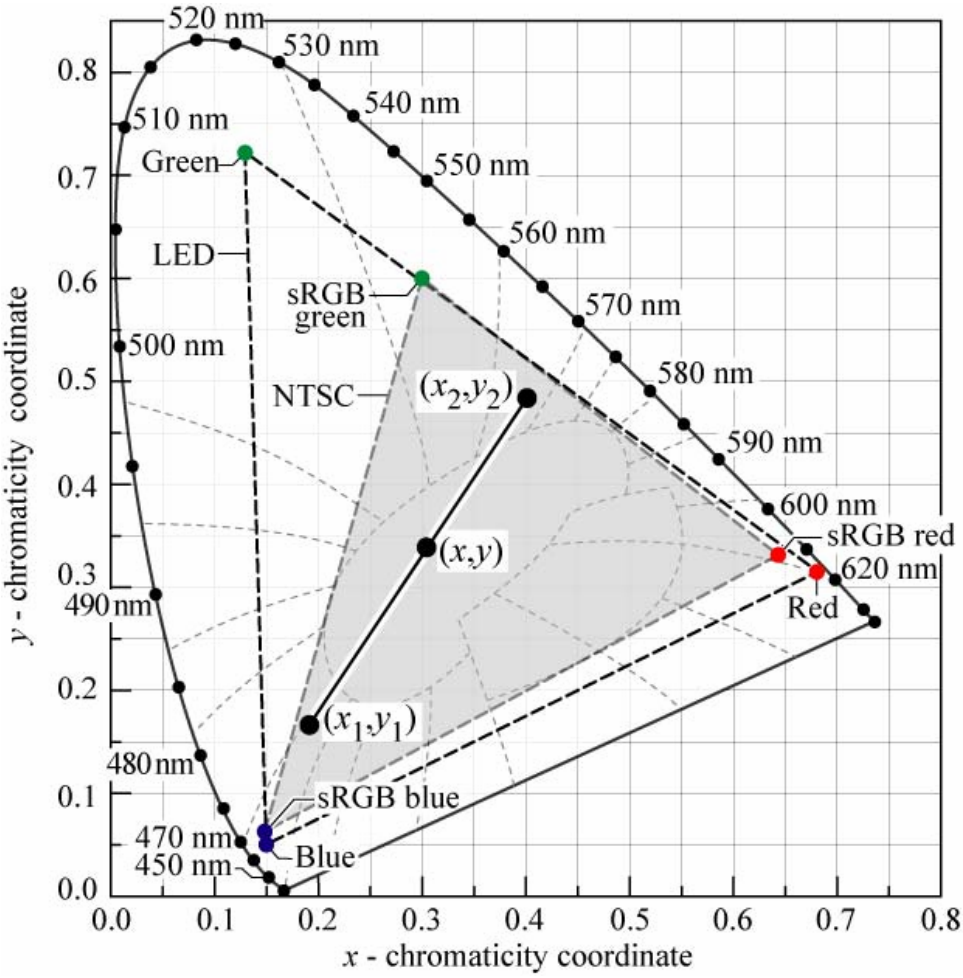

Figure 2.4.1. Principle of color mixing illustrated with two light sources with chromaticity coordinates (x_1,y_1) and (x_2,y_2). Also the triangular area of the

chromatic diagram (color gamut) accessible by additive mixing of a red, green and blue LED is shown (After Ref. 8).

2.5 Color rendering

The ability whether the light sources show the true color of the physical objects is very important. This characteristic of a light source is measured in terms of color-rendering index or CRI. We can see the importance of color rendering in our life, too. The color of objects under high quality white light sources appears richer and more vivid. High color rendering index sources are generally used in museums, homes and offices and low CRI sources mostly used in streets and parking lots.

The color rendering of a test source is measured with respect to a reference light source. In order to calculate the CRI, the reference light source is selected according to the chromaticity coordinate of the test source. If the chromaticity coordinate point is on the planckian locus, the reference source is a planckian blackbody radiator with the same color temperature as the test source. If the coordinate point is off from the planckian locus, the reference source is a planckian black-body radiator with the same correlated color temperature as the test source.

CRI is a unitless quantity that changes form -100 to 100. The reference sources are accepted with a CRI of 100. If a test light source has 100 CRI, then one can understand that the light source is high quality source that can fully render all the colors of the physical objects. Illuminants excluding reference sources generally have CRI lower than 100. Since the CRI is calculated according to the reference source, the selection of the reference source is critically important.

The emission spectrum of incandescent lamp closely follows that of a planckian black-body radiator. Therefore, its CRI is the highest among the artificial sources mentioned in Chapter 1.

To determine the CRI of a test light source additional to the test-color samples, test color samples are needed. In international standardization, 14 test color samples has been agreed in order to measure the CRI, but the general CRI is an average calculated according to the 8 test-color samples with the following formula [8]:

$$CRI_{general} = \frac{1}{8}\sum_{i=1}^{8} CRI_i \tag{2.5.1}$$

The special color-rendering indices are calculated according to:

$$CRI_i = 100 - 4.6\Delta E_i^* \tag{2.5.2}$$

ΔE_i^* is the quantitative color change that occurs when a test-color sample is illuminated with the reference source and then with the test source. The special CRI is 100 if there is no difference of the test-color sample in color under test and reference light source. However, in order to use WLEDs in SSL applications the aim is to have a CRI higher than 80.

Chapter 3

White Light Emitting Diodes

3.1 Working principle of LEDs

By forward biasing the pn junctions electrons and holes are injected into the same region of the semiconductor. As a result they recombine and emit light by spontaneous emission. LEDs can make emission in direct band gap semiconductors and through impurity states [9]. Direct band to band transitions can be made in any direct band gap material and combinations of materials that have hole and electron wavefunction overlap under forward bias. Emission through impurity states can be made in different ways: donor state to valence band, conduction state to acceptor state and donor state to acceptor state.

Because of the wide range of available direct gap semiconductors and impurity states in indirect semiconductors, there is broad range of spectral range that can be covered form infrared to ultraviolet. Some possible semiconductor materials and wavelengths are listed in Table 3.1.1. Wide range of available wavelengths for LEDs with different combination of luminescent materials make possible to produce white light generation.

Material	Wavelength (nm)
InAsSbP/InAs	4200
$In_{0.53}Ga_{0.37}As$	1550
GaAs:Si	940
GaP	690
SiC	400-460

Table 3.1.1. Materials and their emission wavelengths [After Ref. 9].

3.2. White LEDs

There is an increasing research effort in the development of general daylight illumination devices because of the huge market size and application such as in homes, cars, offices, and so on. The general daylight illumination systems should have the following properties [8]:

- high efficiency
- high power capability
- good color rendering capabilities
- high reliability
- low-cost manufacturability
- environmental friendly

These properties would give the opportunity WLEDs to compete with other light sources. Although LEDs are commonly monochromatic sources, there are mainly three ways for making white LEDs: multichip white LEDs, monolithic white LEDs and color conversion based WLEDs.

3.2.1 Multichip white LEDs

In this approach multiple emitter diodes are mounted in one package. Multichip white LEDs have three individual LEDs, which are generally InGaN based blue- and green-LEDs, and an AlGaInP based red-LED [10].

3.2.2. Monolithic white LEDs

This second method for white light generation is monolithic white LED method which relies on using the multicolor emitting multiple-quantum well (MQW) for the active layers. Generally these LEDs use several InGaN active layer and cover a visible region with high color purity. The Figure 3.2.2.1 shows the epitaxial design of such a monolithic white LED.

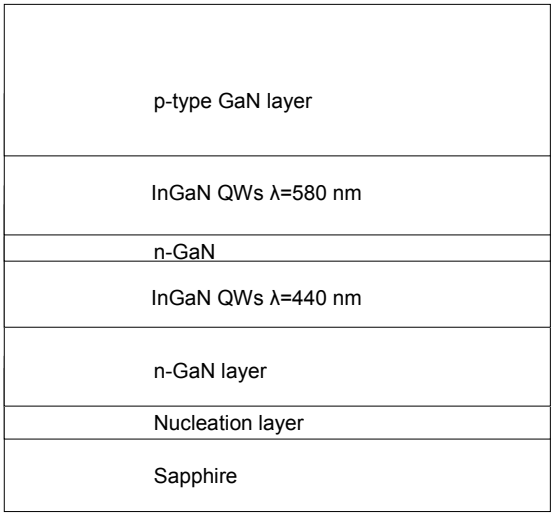

Figure 3.2.2.1. An epitaxial design example of monolithic white LEDs.

3.2.3 WLEDs based on wavelength converters

As the third method, we look at the color conversion method. There are different materials which can be used as wavelength converters (dyes, polymers, phosphors and nanocrystals) and these materials are integrated on the LEDs. The operating principle of these hybrid WLEDs relies on the hybrid use of the LED as the pump light source and the integrated film consisting of the wavelength converter materials as the photoluminescent layer. When electrically driven, the LED optically pumps the wavelength converter materials. The photoluminescence of these materials and the electroluminescence of the LED consequently contribute together to the white light generation.

3.2.3.1 Dye based WLEDs

Many different dyes for instance Coumarin 6 can have very high quantum efficiency close to %100 [8]. But they have long-term stability problem that prevent them to be used as a commercial product in white LEDs. After some number of photon absorption events, dye molecules become optically inactive; in other words, they bleach out.

3.2.3.2 Polymers based WLEDs

Among various polymer types, specifically conjugated polymers can be one of the strong candidates in lighting applications. They have very strong absorption both in n-UV and blue on the order of 10^5 cm^{-1} with very high quantum efficiency which is better than phosphors; additionally they can deposited easily

with common techniques such as dipping and spin coating and noticably they are almost entirely free from concentration quenching effects [11]. Some polymers also have long-term stability problem which can be a strong obstacle for commercial application.

3.2.3.3 Phosphors based WLEDs

Phosphors consist of an inorganic host material commonly garnets doped with an optically active element. Phosphors with yttrium aluminum garnet (YAG) are the most widely used host material. The optical characteristics of YAG phosphor can be changed by substituting Gadolinium (Gd) for Yttrium (Y),Gallium (Ga) for Aluminum (Al) and doping with cerium (Ce) whose chemical formula is $(Y_{1-a}Gd_a)(Al_{1-b}Ga_b)_5O_{12}$: Ce [8].

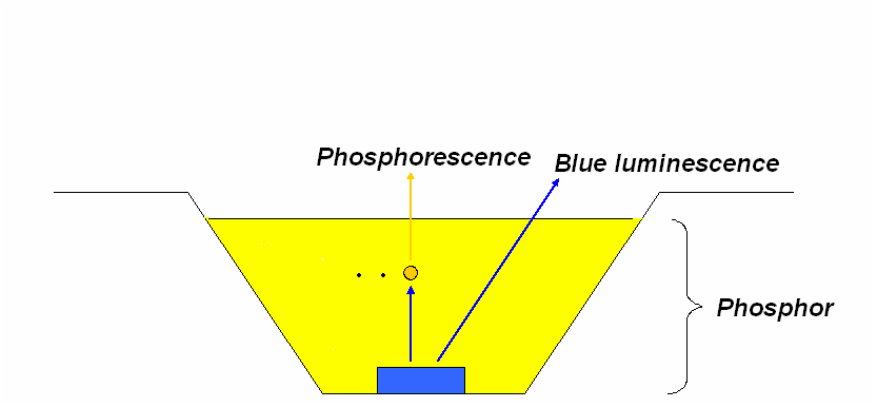

Figure 3.2.3.3.1. Wavelength-converting phosphorescence and blue luminescence in phosphor based WLEDs.

3.2.3.3.1 Blue-pumped phosphor based white LEDs

After Nakamura et al. reported the InGaN/GaN LED that can generate 3 mW optical power (1995), Bondo et al. used phosphor wavelength converter on InGaN/GaN blue LED [12,13]. Afterward Nichia Corporation commercialized for the first time the blue InGaN/GaN LED and phosphor based white LEDs which integrated on the blue InGaN/GaN LED. These historical points in the history can be accepted as the turning point of the solid state lighting dream which longs for LEDs to be used for every illumination need.

Blue-pumped phosphor based white LEDs are schematically as shown in Figure 3.2.3.3.1. The cup shaped depression is filled with the phosphor resin where at the bottom the LED die stands. Some portion of the blue light coming from the electroluminescence (EL) is absorbed by the phosphor and the rest transmits. After absorption the phosphor makes photoluminescence (PL), and the EL and PL generates white light together. The optical properties of WLED are determined by the thickness and concentration of the phosphor resin.

3.2.3.3.2 UV-pumped phosphor based white LEDs

WLEDs can be also achieved by using ultraviolet (UV) source as well. The UV light pumps the phosphor and the entire visible spectrum is covered by the PL of phosphors. The UV pump source can be selected from near UV (320 nm-390 nm) to deep UV (320 nm-210 nm). But as the pump source goes to deeper UV, the energy loss because of the conversion from UV to visible increases. In Table 3.2.3.3.2.1 presents a comparison of advantages and disadvantages among blue-

pumped phosphor based white LEDs, UV-pumped phosphor based white LEDs and multichip WLEDs [10,14].

	Advantages	**Disadvantages**
Blue-pumped phosphor based white LEDs	- Most mature technology - High-volume manufacturing processes - Relatively high luminous flux - Relatively high efficacy - Comparatively lower cost	- High CCT (cool/blue appearance) - Low CRI (typically in the 70s) - Color variability in beam - Difficulties in controlling granule size systematically and mixing and depositing films uniformly
UV-pumped phosphor based white LEDs	- Higher color rendering - Warmer color temperatures possible - Color appearance less affected by chip	- Less mature technology - Relatively low efficacy - Relatively low light output - the low absorption of phosphors at near-ultraviolet (n-UV) wavelengths results in small

	variations	conversion efficiencies - Difficulties in controlling granule size systematically and mixing and depositing films uniformly
Multichip-white-LEDs	- Color flexibility, both in multi-color displays and different shades of white - Potentially very high color rendering	- Individual colored LEDs respond differently to drive current, operating temperature, dimming, and operating time - Controls needed for color consistency add expense -Complex driving circuitry
Monolithic-white-LEDs	- Simple circuitry - Potentially high color rendering	- the EL peaks very sensitive to LED temperature (change of optical properties with temperature) - forward bias current changes the color temperature

Table 3.2.3.3.2.1. Comparison of current white LED technologies.

Chapter 4

Nanocrystals

Quantum dots are nanosize crystals composed of periodic groups of II-VI, III-V, or IV-VI materials. In such nanocrystals, the atoms form together sphere like structure whose diameters range from 2-10 nanometers. The nanocrystals (NCs) emission can be tuned by dot size and composition. In the bulk case, the energy levels in valence and conduction bands are continous. However, as the size of the crystal decreases, the continous energy levels start to discretize. In other words, when the nanorystals begin to be synthesized smaller than the Bohr radius, the quantum size effect (quantum confinement) begin to be observed. By using the size effect, the NCs emission peak can be tuned. If this band gap energy corresponds to the photons in visible, the color of the emission of NCs perceived by the human eye can be tuned. For instance, CdSe/ZnS core-shell nanocrystals having 4.2 nm diameter have luminescence at green and the same type of nanocrystals having 5.7 nm diameter have red luminescence. Another degree of freedom though which the emission peak of nanocrystals can be tuned is the composition of nanocrystals. By using various materials the band gap energy of the NC can be adjusted and emission wavelenghts from violet to mid-infrared across the whole spectrum can be achieved. For example, by using

CdSe/ZnS core shell nanocrystals most of the visible spectrum from 490 nm to 620 nm can be covered and by using PbSe and PbS the emission peak in the near infrared spectrum can be adjusted from 850 to 2100 nm [15].

4.1 Synthesis of Nanocrystals

The NCs can be synthesized with the hot injection method. To synthesize CdSe core NCs, we need 1 gr HdA, 1 gr TOPO, 6 ml octadecene, 2 ml Cd solution [0.1 Molar]. We put all of them into the flask as in Figure 4.1.1 and heat it to 280^{o} C.

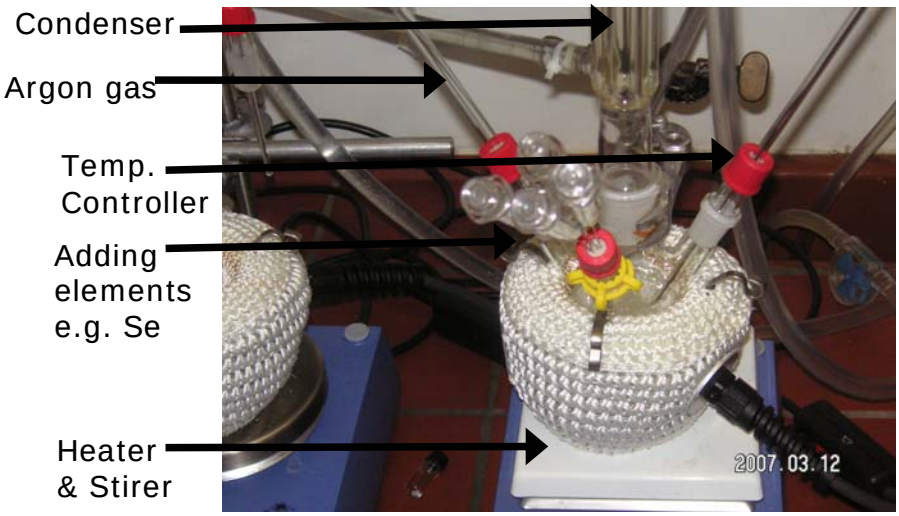

Figure 4.1.1. Photograph of nanocrystal synthesis flask with the necessary equipments with their explanation.

Afterward we add Se solution. However, transfering Se and putting it into the flask is a dangerous task because it should not get in touch with oxygen.

Therefore, it is taken into in glove box in Figure 4.1.2 where there is no oxygen. As soon as, we inject 2 ml 0.1 Molar Se solution into the flask, the reaction starts.

Figure 4.1.2. Photograph of glove box used for taking Se solution.

The reaction time and reaction temperature determine the size of the core NCs and therefore the emission wavelength. At 280^{o} C 5 seconds or less reaction time results cyan emitting NCs and 5 minute or more reaction time causes red emitting NCs. At higher reaction temperatures less than 5 minutes is sufficient for obtaining red NCs. After the reaction time finished, we cool the flask by putting it into a water cup at room temperature. We add hexane solution and put into another clean flask. We wait a few hours for NCs and hexane solution phase separation and finally we take the NCs into the tubes. The photographs of NCs under UV light are shown in Figure 4.1.3.

Figure 4.1.3. Photograph of cyan, green, and red CdSe core NCs and surface state emtting CdS NCs (from right to left).

4.2 Synthesized nanocrystals and their photoluminescence peaks

Table 4.2.1 displays the photoluminescence peaks and materials of NCs that we synthesized as a collaborative research effort between Bilkent University and Technical University of Dresden within EUFP6 Phoremost Network of Excellence. Figure 4.2.1-10 shows the normalized absorption and emission spectra of synthesized NCs which are given in Table 4.2.1.

Nanocrystal	**PL peak (in solution)**
CdS	419
CdS	445
CdSe	456
CdSe	485

CdSe	502
CdSe	521
CdSe	538
CdSe	620
CdS (surface state emitting NCs)	emission across the entire visible
CdSe/ZnS/CdSe (onion-like NCs)	520-560-620

Table 4.2.1. The types nanocrystals and the photoluminescence peak of synthesized nanocrystals.

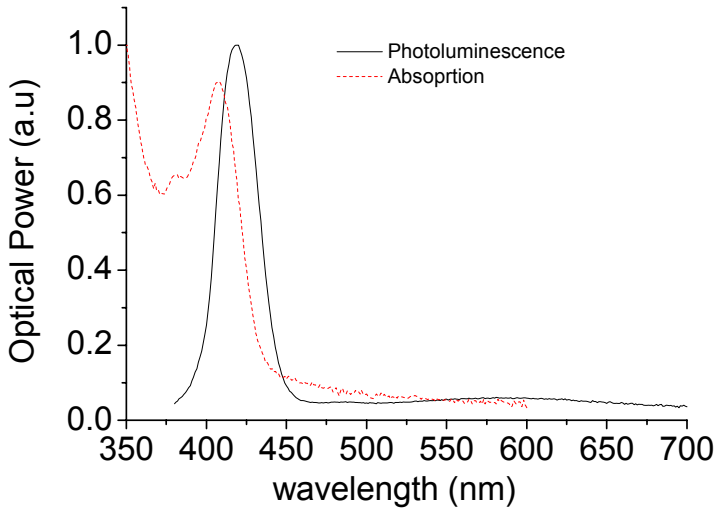

Figure 4.2.1. PL and absorption spectra of violet (λ_{PL}=419 nm) CdS nanoparticle in solution.

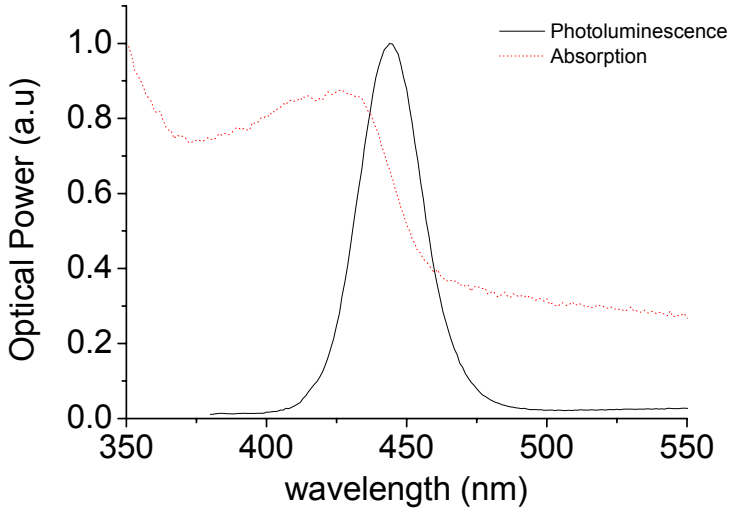

Figure 4.2.2. PL and absorption spectra of blue CdS (λ_{PL}=445 nm) nanoparticle in solution.

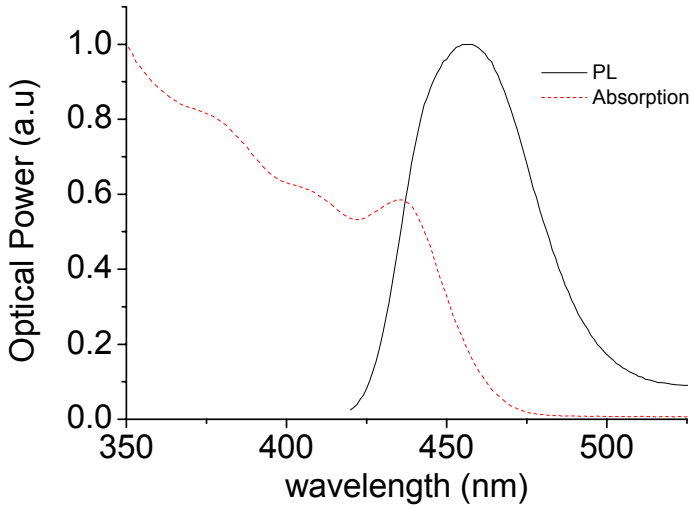

Figure 4.2.3. PL and absorption spectra of blue (λ_{PL}=456 nm) CdSe nanoparticle in solution.

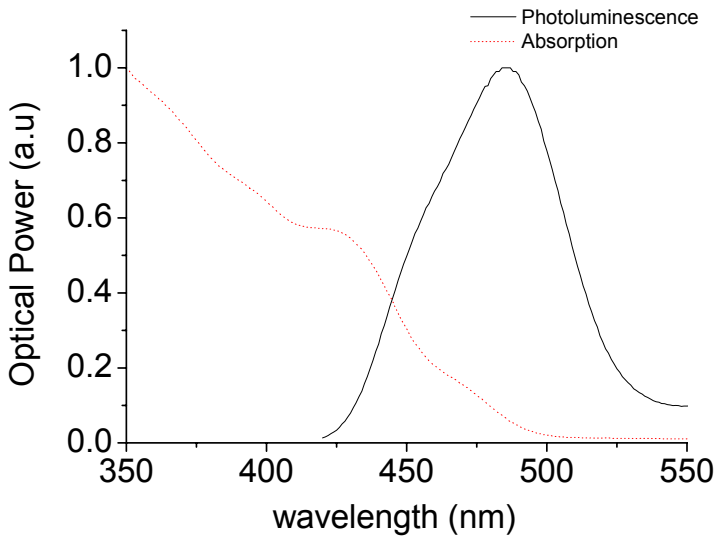

Figure 4.2.4. PL and absorption spectra of CdSe (λ_{PL}=485 nm) nanoparticle in solution.

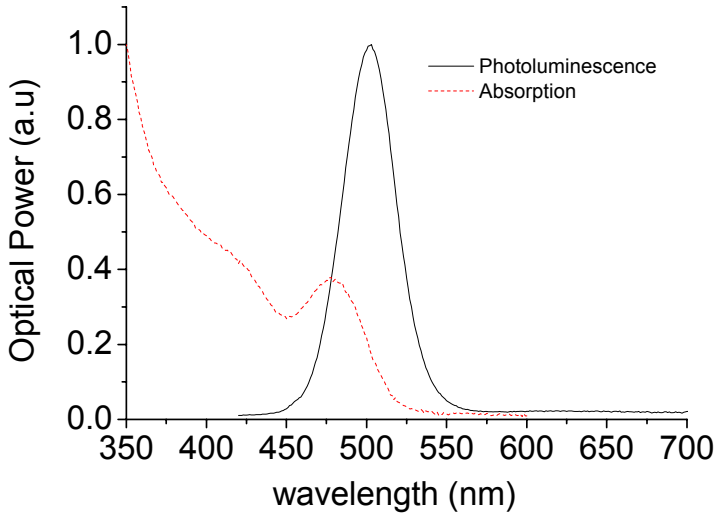

Figure 4.2.5. PL and absorption spectra of cyan CdSe (λ_{PL}=502 nm) nanoparticle in solution.

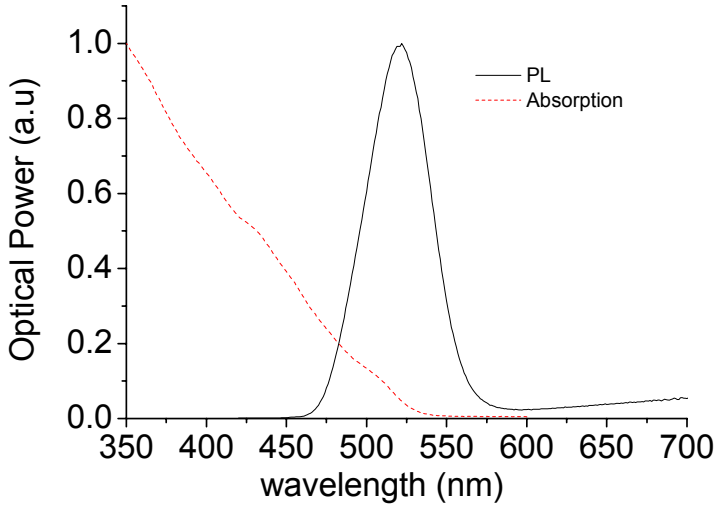

Figure 4.2.6. PL and absorption spectra of green (λ_{PL}=521 nm) CdSe nanoparticle in solution.

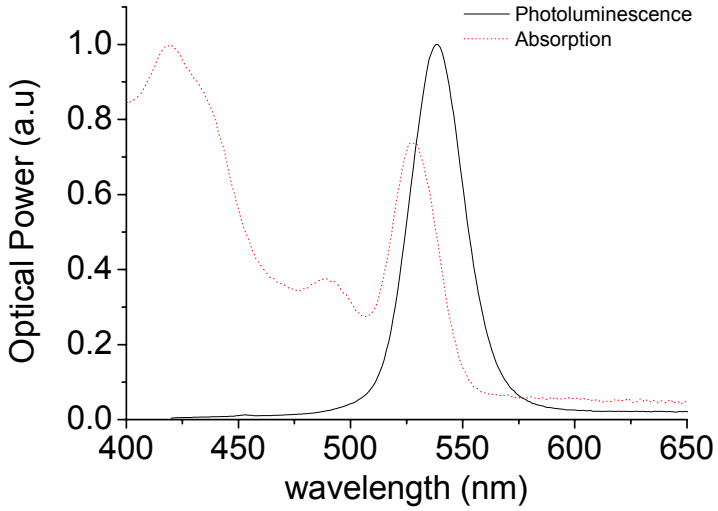

Figure 4.2.7. PL and absorption spectra of yellow CdSe (λ_{PL}=538 nm) nanoparticle in solution.

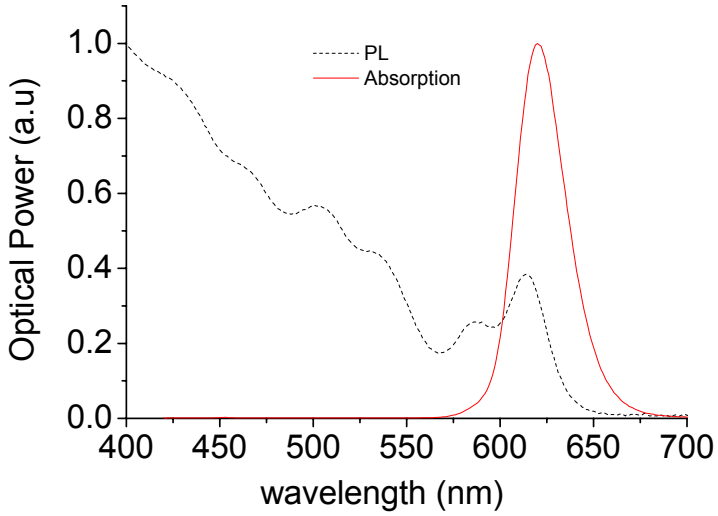

Figure 4.2.8. PL and absorption spectra of red (λ_{PL}=620 nm) CdSe nanoparticle in solution.

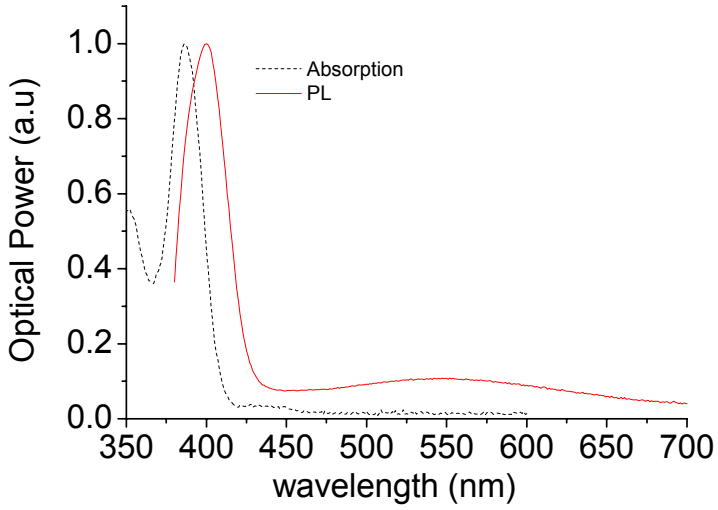

Figure 4.2.9. PL and absorption spectra of white surface state emitting CdS nanoparticle in solution.

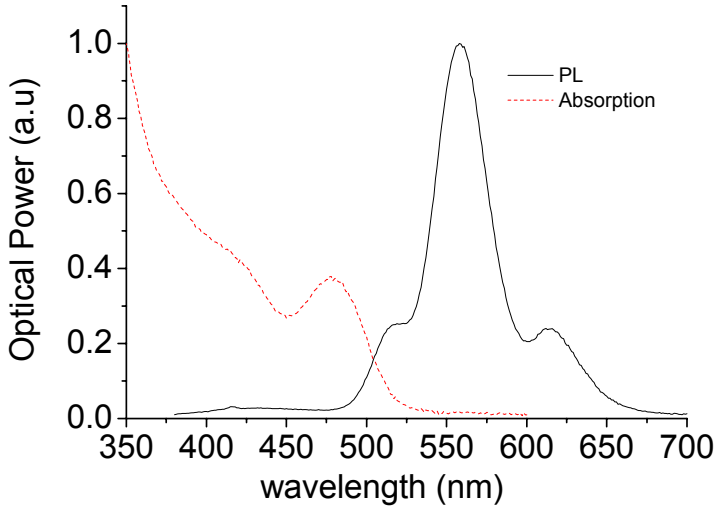

Figure 4.2.10. PL and absorption spectra of onion like CdSe/ZnS/CdSe (λ_{PL}=520, 560 and 620 nm) nanoparticle in solution.

4.3 Theoretical investigation of energy levels

The stationary Schrödinger equation for a particle under the action of a force can be expressed as:

$$\left[-\frac{\hbar^2}{2m}\nabla^2 + V(\vec{r})\right]\psi(\vec{r}) = E\psi(\vec{r}) \qquad (4.3.1)$$

where $\hbar$ is Planck's constant divided by 2π, m is the particle mass, $V(\vec{r})$ is the potential, E is the energy eigenvalue and $\psi(\vec{r})$ is the eigenfunction. For a spherically symmetric potential $V(\vec{r}) = V(r)$ and the wavefunction can be separated to its radial and angular parts,

$$\psi_{nlm}(r,\theta,\phi) = R_{nl}(r)Y_{lm}(\theta,\phi) \qquad (4.3.2)$$

$R_{nl}(r)$ is the radial wavefunction, $Y_{lm}(\theta,\phi)$ is the spherical harmonic, n is the principal quantum number, and l and m are the angular momentum numbers. The spherical potentials in different N regions can be written as

$$V(r)=\begin{cases} V_1 & \text{for } 0 \le \mathrm{r} < r_1 \\ V_2 & \text{for } \mathrm{r}_1 \le \mathrm{r} < r_2 \\ . & \\ . & \\ V_N & \text{for } \mathrm{r}_{N\text{-}1} \le \mathrm{r} < \infty \end{cases} \tag{4.3.3}$$

The radial eigenfunction can be $R_{nl}(r)$ written as

$$R_{nl}(r)=\begin{cases} R_{nl,1} & \text{for } 0 \le \mathrm{r} < r_1 \\ R_{nl,2} & \text{for } \mathrm{r}_1 \le \mathrm{r} < r_2 \\ . & \\ . & \\ R_{nl,N} & \text{for } \mathrm{r}_{N\text{-}1} \le \mathrm{r} < \infty \end{cases} \tag{4.3.4}$$

If we look at the solution of $R_{nl,q}$ when $E_{nl} > V_q$, the solution is a linear combination of spherical Bessel and Neumann functions j_l and n_l, respectively:

$$R_{nl,q}(r) = A_{nl,q} j_l(k_{nl,q} r) + B_{nl,q} n_l(k_{nl,q} r) \tag{4.3.4}$$

where

$$k_{nl,q} = \left[\frac{2m_q (E_{nl} - V_q)}{\hbar^2} \right]^{1/2} \tag{4.3.6}$$

and m_q is the effective mass of a particle in region q.

If we look at the solution of $R_{nl,q}$ when $E_{nl} < V_q$, the solution is a linear combination of two Hankel functions $h_l^{(+)}$ and $h_l^{(-)}$ [16]:

$$R_{nl,q}(r) = A_{nl,q} h_l^{(+)}(iK_{nl,q} r) + B_{nl,q} h_l^{(-)}(iK_{nl,q} r) \tag{4.3.7}$$

where

$$K_{nl,q} = \left[\frac{2m_q (V_q - E_{nl})}{\hbar^2} \right]^{1/2} \tag{4.3.8}$$

The solution should satisfy the continuity at boundary conditions for each part

$$R_{nl,q}(r_q) = R_{nl,q+1}(r_q) \tag{4.3.9}$$

$$\frac{1}{m_q} \frac{dR_{nl,q}(r)}{dr}\bigg|_{r=r_q} = \frac{1}{m_{q+1}} \frac{dR_{nl,q+1}(r)}{dr}\bigg|_{r=r_q} \tag{4.3.10}$$

The solution has to be regular at r = 0 and R_{nl} should go to zero when $r \to \infty$. In this solution, since we have N parts, we have 2N unknowns. As a result of continuity at boundaries, we have 2N-2 equations because we have N-1 boundaries. We need two equations more to completely solve the coefficients. One of them is that the determinant of the coefficients should be zero to have a solution $D_l = D_l(E_{nl}) = 0$. Another one is the normalization condition for $R_{nl}(r)$. Since we need to calculate the interband transitions from conduction band to valence band, we can only look at 1s states both for electrons and holes in which n=1, l=0, m=0 and $Y_{0,0}(\theta,\phi)$ yields a constant factor of $1/(4\pi)^{1/2}$. We perform the calculations for electrons and holes separately because their band discontinuities and effective masses are generally different.

4.4 Calculation of energy eigenvalues and energy eigenfunctions of CdSe/ZnS core-shell nanocrystals

The material parameters of CdSe and ZnS are given in Table 4.4.1. By using these parameters, the radial energy diagram of CdSe/ZnS core-shell nanocrystal is as given in Figure 4.4.1

Material	m_e^*	m_h^*	E_g (eV)	E_{vacuum} (eV)
CdSe	0.13	0.45	1.7	4.4
ZnS	0.28	0.49	3.76	3.4

Table 4.4.1. Material parameters of CdSe and ZnS [After Ref. 17, 18].

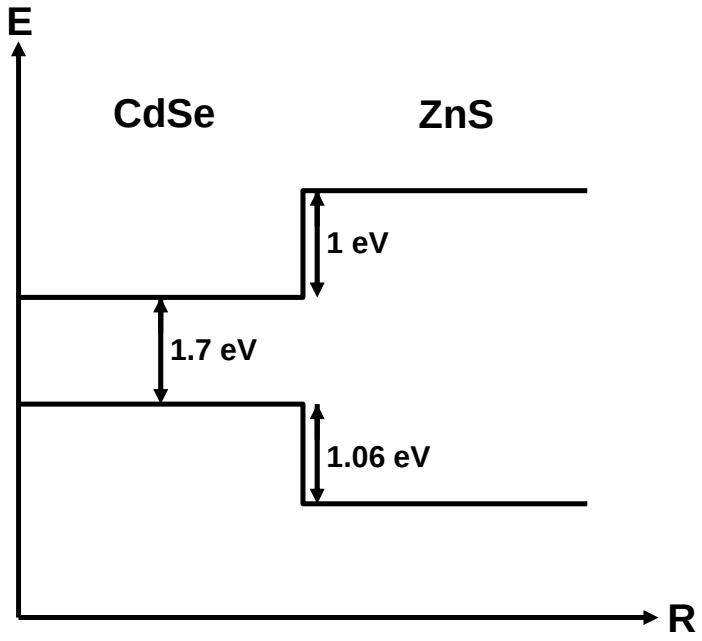

Figure 4.4.1. Energy diagram of CdSe/ZnS core-shell nanocrystals.

Since in bound states $E_{nl}>V_q$, the general wavefunction in CdSe well should consist of linear combinations of spherical Bessel and Neumann functions. The

wavefunction should not blow up at r=0, so the coefficient of Neumann function should be zero. Therefore, the wavefunction has the following form:

$$\psi_1(r) = A\frac{\sin(k_1 r)}{k_1 r} \tag{4.4.1}$$

In ZnS barrier, because of $E_{nl}<V_q$, the general wavefunction can be written as a linear combination of spherical Hankel functions. Since the wavefunction in barrier should vanish as $r \to \infty$, it is of the form of:

$$\psi_2(r) = B\frac{e^{-k_2 r}}{k_2 r} \tag{4.4.2}$$

The k_q's can be written in terms of energy as

$$k_1 = \sqrt{\frac{2m_{1,eff}E}{\hbar^2}} \tag{4.4.3}$$

because V_1 is zero.

$$k_2 = \sqrt{\frac{2m_{2,eff}(V_2 - E)}{\hbar^2}} \tag{4.4.4}$$

We can write the following equalities at boundaries between core and shell,

$$A\frac{\sin(k_1 d)}{k_1 d} = B\frac{e^{-k_2 d}}{k_2 d} \tag{4.4.5}$$

$$\frac{A}{m_{1,eff}}\left[\frac{\cos(k_1 d)}{d} - \frac{\sin(k_1 d)}{k_1 d^2}\right] = \frac{B}{m_{2,eff}}\left[-\frac{e^{-k_2 d}}{d} - \frac{e^{-k_2 d}}{d^2}\right] \tag{4.4.6}$$

Then we should write these equations in the 2x2 matrix form. We have solution when the determinant of the matrix (which is dependent on k_1 and k_2 in other words energy) is zero. At the first energy value that crosses zero is our E_{1s} energy eigenvalue. For one computational example, we take the crystal diameter to be 4.8 nm (d=2.4) whose PL is provided in Reference 21 so that we can also compare our results. The determinant vs. energy for electrons is given in Figure 4.4.2.

The zero-crossing energy with respect to its conduction band is

$$E_{1se}= 0.2686 \text{ eV} \qquad (4.4.7)$$

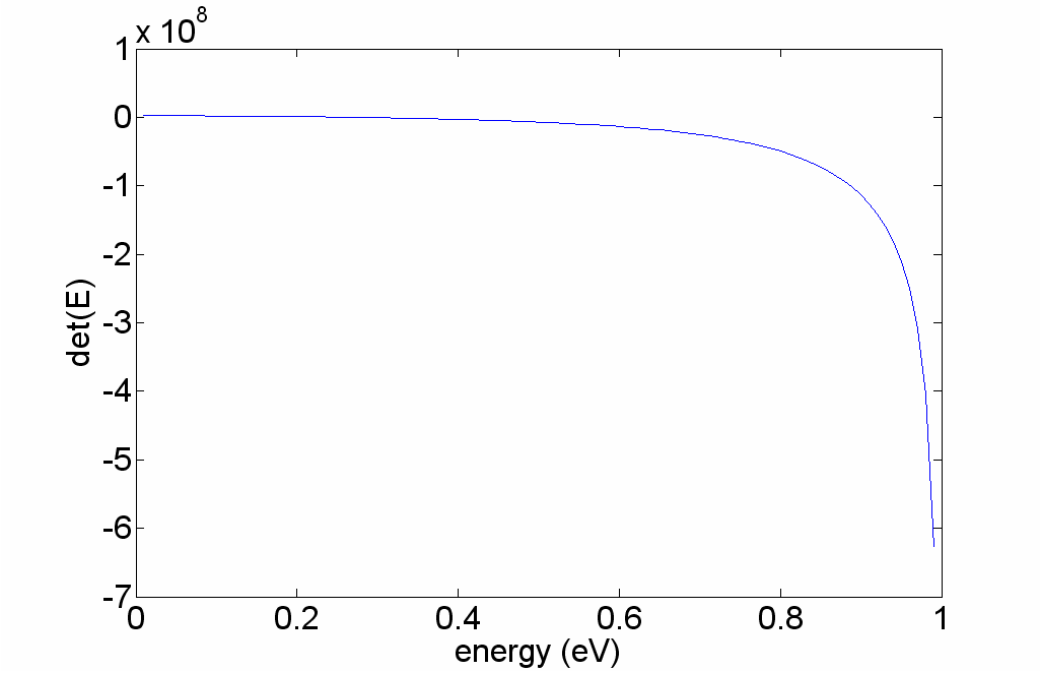

Figure 4.4.2. Determinant of 2x2 matrix vs. energy for electrons.

The determinant vs. energy for holes is plotted in Figure 4.4.3. The zero-crossing energy for holes with respect to valence band is

$$E_{1sh}=0.1143 \text{ eV} \qquad (4.4.8)$$

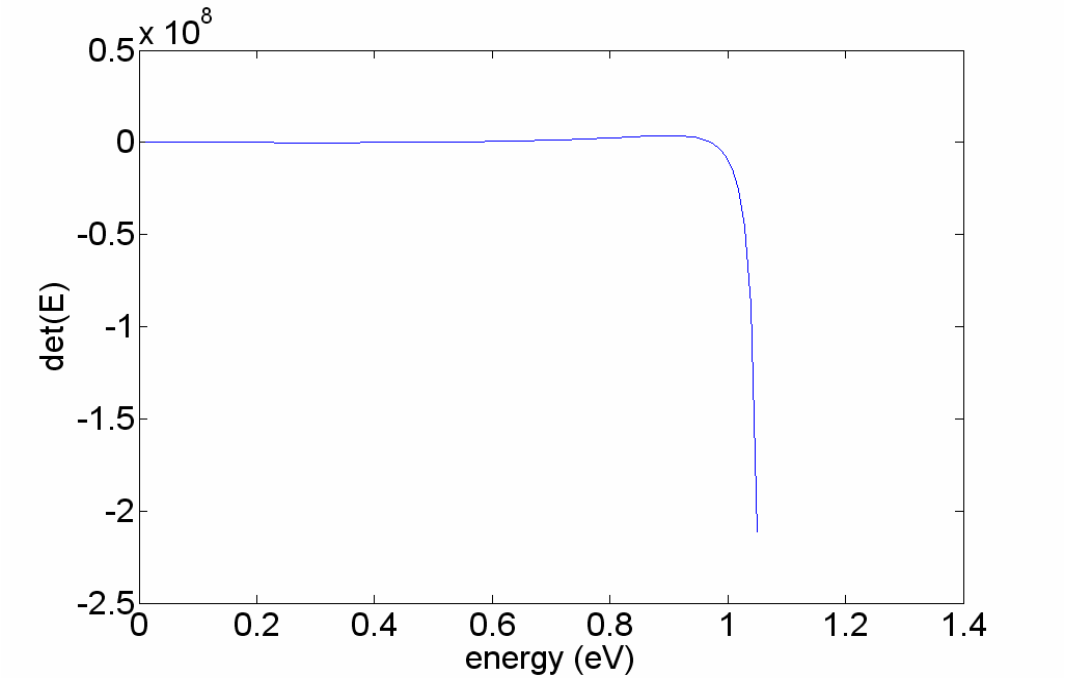

Figure 4.4.3. Determinant of 2x2 matrix vs. energy for holes.

The total energy difference is then

$$\Delta E = E_g(CdSe) + E_{1se} + E_{1sh} = 1.70 + 0.2686 + 0.1143 = 2.0803 \text{ eV} \qquad (4.4.9)$$

The corresponding wavelength is

$$\lambda \cong 596 \text{ nm} \qquad (4.4.10)$$

The measured photoluminescence in [12] is approximately 598 nm, which shows that our theoretical calculations fit very well to the experimental data.

If we find the electron probability distribution:

$$B/A = -472.9965 \qquad (4.4.11)$$

$$k_1 = 9.5778 \times 10^8 \text{ 1/m} \qquad (4.4.12)$$

$$k_2 = 2.3195 \times 10^9 \text{ 1/m} \qquad (4.4.13)$$

By using normalization,

$$A = 8.541 \times 10^{13}\ 1/m^{1/2} \quad (4.4.14)$$

$$B = -4.04 \times 10^{16}\ 1/m^{1/2} \quad (4.4.15)$$

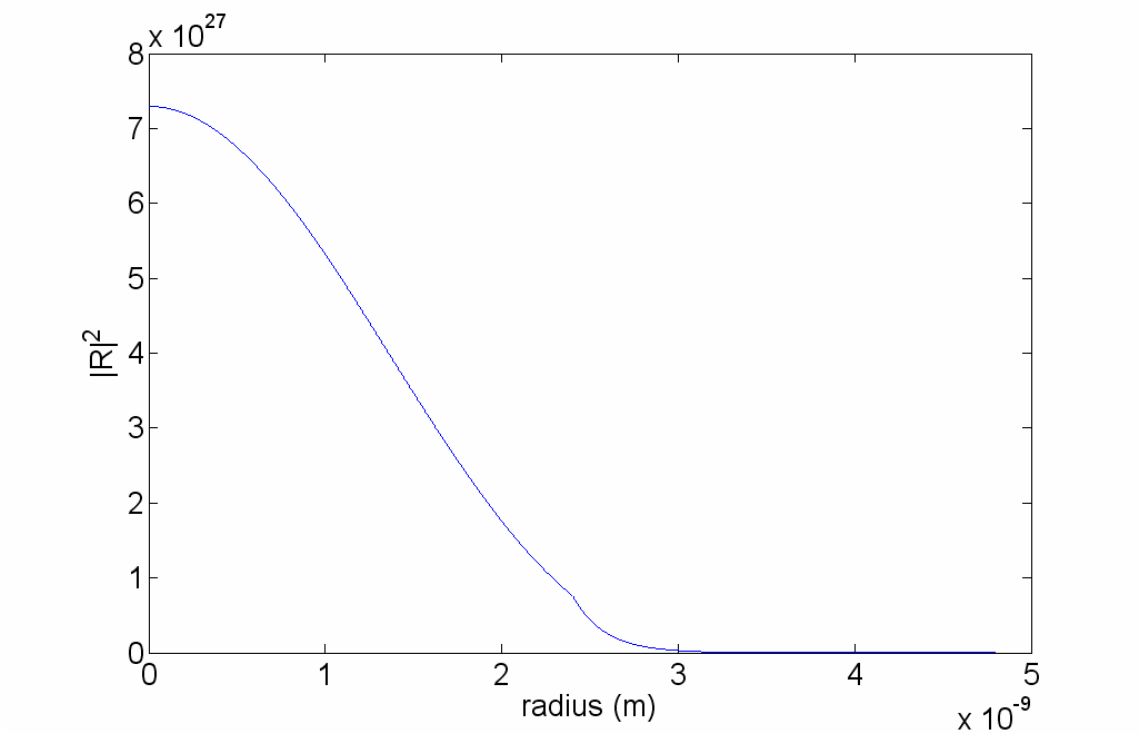

Figure 4.4.4. Radial probability distribution of electrons.

If we find the hole probability distribution,

$$B/A = -4.4803 \times 10^{3} \quad (4.4.16)$$

$$k1 = 1.1624 \times 10^{9} \quad (4.4.17)$$

$$k2 = 3.4891 \times 10^{9} \quad (4.4.18)$$

By using normalization,

$$A = 1.118 \times 10^{14}\ 1/m^{1/2} \quad (4.4.19)$$

$$B = 5.006 \times 10^{14}\ 1/m^{1/2} \quad (4.4.20)$$

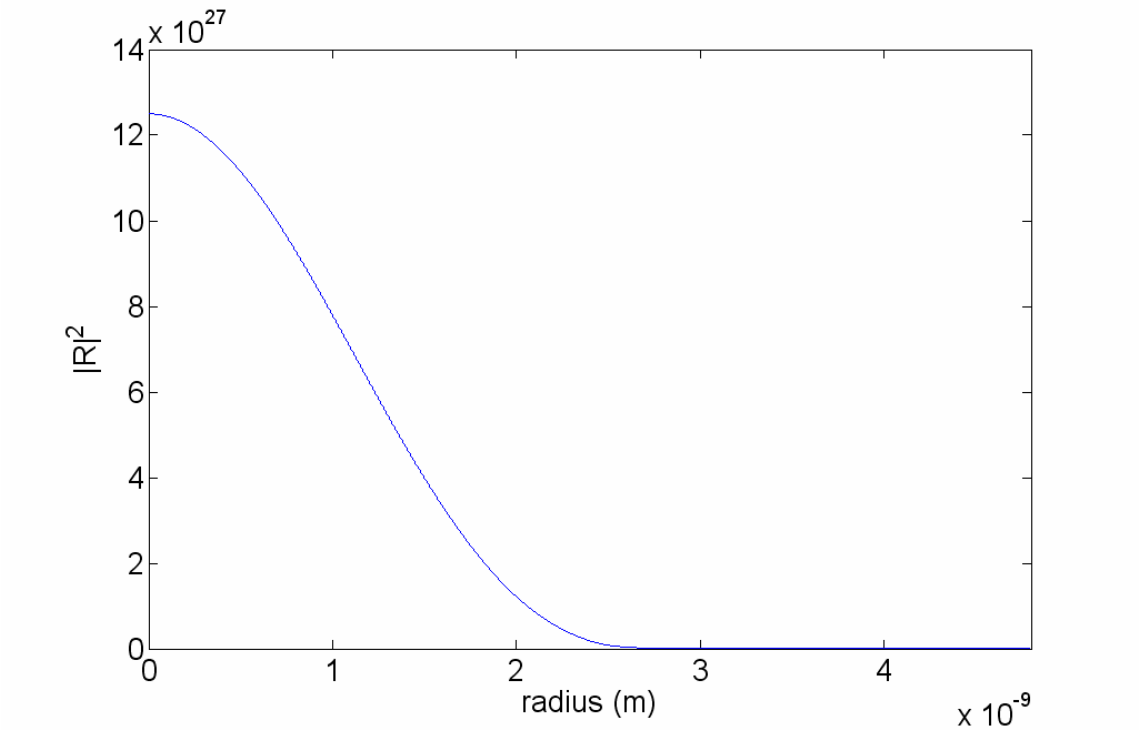

Figure 4.4.5. Radial probability distribution of holes.

From here we see that although electron and holes are more concentrated on the core, they also slightly penetrate to the barrier as well. Since its effective mass is smaller, the electron can penetrate more into the barrier. As Battaglia et al. explained in [19] after the third monolayer of ZnS barrier, the carriers become isolated in the nanocrystal (but not for one and two monolayer barriers). Adding three monolayers of ZnS shell corresponds to 1.6 nm thickness [20]. If we look at the probability distributions of holes, we observe that the hole distribution vanishes almost when it reaches 2.8 nm. Additionally, if we look at the probability distributions of electrons, their probability vanishes approximately at 3.4 nm. Therefore, we conclude that one or two monolayers of ZnS barriers do not fully isolate the carriers in quantum dot, but three monolayers of ZnS barrier

confines the carriers as discussed in [19]. Also we make calculations for nanocrystals of different sizes; the comparison is shown in Table 4.4.2.

NC core diameter size (nm)	**2.3**	**4.2**	**4.8**	**5.5**
Experimental PL data (nm) [21]	480	568	598	624
Calculated PL data (nm)	450	572	595	617

Table 4.4.2. Experimentally measured and theoretically calculated PL peaks for different-size CdSe/ZnS core-shell nanocrystals.

Except the results for nanocrystal with 2.3 nm radius, the other results are compromising. The discrepancy for the nanocrystal with 2.3 nm radius can be attributed to the excitonic effects. Since the carriers are more confined in a tighter volume, the Coulomb interaction between the electron and hole will be more significant, introducing excitonic states and further decreasing the energy separation between the electron and hole energy levels.

Chapter 5

Nanocrystals based hybrid LEDs to generate and tune white light

5.1 White light generation using CdSe/ZnS core–shell nanocrystals hybridized with blue InGaN/GaN light emitting diodes

To date multi-chip WLEDs, monolithic WLEDs, and color-conversion WLEDs, commonly with phosphor, have been extensively exploited [8,10,22]. Also, as an alternative approach, nanocrystals (NCs) have recently been used for color conversion in white light generation; a blue/green two-wavelength InGaN/GaN LED coated with a single type of red NC and a blue InGaN/GaN LED with a single type of yellow NC and a dual type of red and green NCs have been reported [23-25].

In the most common approach of color-conversion WLEDs coated with phosphor, although phosphor is good for photoluminescence across the visible, in addition to its disadvantages explained in Table 3.2.3.3.2.1, it has a fixed

emission spectrum. On the other hand, the use of combinations of nanocrystals provides the ability to easily adjust the white light parameters. Therefore, in this part, we introduce white light generation using CdSe/ZnS core-shell nanocrystals of single, dual, trio, and quadruple combinations hybridized with InGaN/GaN LEDs as shown in Figure 5.1.1 while generating white light.

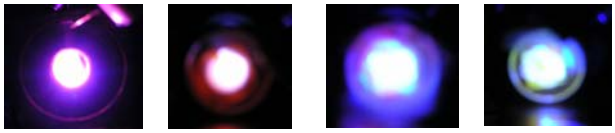

Figure 5.1.1. Photographs of our white hybrid NC-WLEDs while emitting white light: (a) yellow NCs (λ_{PL}=580 nm) hybridized with blue LED (λ_{EL}=440 nm), (b) cyan and red NCs (λ_{PL}=500 nm and 620 nm) with blue LED (λ_{EL}=440 nm), (c) green, yellow, and red NCs (λ_{PL}=540 nm, 580 nm and 620 nm) with blue LED (λ_{EL}=452 nm), and (d) green, cyan, yellow, and red NCs (λ_{PL}=500 nm, 540 nm, 580 nm, and 620 nm) with blue LED (λ_{EL}=452 nm).

We present the design, growth, fabrication, and characterization of our white hybrid nanocrystal-LEDs that incorporate combinations of *1.)* yellow nanocrystals (λ_{PL}=580 nm) on a blue LED (λ_{EL}=440 nm) with tristimulus coordinates of (x, y)=(0.37, 0.25), correlated color temperature of T_c=2692 K, and color rendering index of R_a=14.69; *2.)* cyan and red nanocrystals (λ_{PL}=500 nm and 620 nm) on a blue LED (λ_{EL}=440 nm) with (x, y)=(0.37, 0.28), T_c=3246 K, and R_a=19.65; *3.)* green, yellow, and red nanocrystals (λ_{PL}=540 nm, 580 nm, and 620 nm) on a blue LED (λ_{EL}=452 nm) with (x, y)=(0.30, 0.28), T_c=7521 K, and R_a=40.95; and *4.)* green, cyan, yellow, and red nanocrystals (λ_{PL}=540 nm, 500 nm, 580 nm, and 620 nm) on a blue LED (λ_{EL}=452 nm) with (x, y)=(0.24, 0.33), T_c=11171 K, and R_a= 71.07 [26,27].

5.1.1 The operating principle

The operating principle of these hybrid NC-WLEDs relies on the hybrid use of the LED as the pump light source and the integrated NC film as the photoluminescent layer. When electrically driven, the LED optically pumps the NCs. The photoluminescence of these NCs and the electroluminescence of the LED consequently contribute together to the white light generation. Here with the ability to tune the NC photoluminescence peaks across the visible (using the size effect) and with the right choice of NC combinations, we cover the visible spectrum from blue to red with a necessary spectral power distribution. Furthermore, with the small overlap between the NC emission and absorption spectra, we conveniently modify the white light spectrum as desired with the addition of NCs.

5.1.2. Device parameters

To adjust the optical properties of the generated white light, we carefully set the device parameters including the type and density of NCs and the thickness and order of the NC films. The type of NCs determines the intervals of the visible spectrum designed to contribute to white light. The NC density and the film thickness affect the level of conversion from incident photons to emitted/transmitted photons for each NC layer. The order of NC films, with a different NC type in each film, sets the level of reabsorption of the photons emitted by the preceding NC layers. Therefore, the ability to control such hybrid

device parameters makes it possible to generate the intended white light spectrum.

5.1.3. Nanocrystals

We use four types of CdSe/ZnS core-shell NCs with their photoluminescence in the visible spectral range of cyan, green, yellow, and red from Evident Technologies. The NC diameters and their corresponding peak photoluminescence wavelengths are provided in Table 5.1.3.1. We use these NCs blended in host resin with a size distribution of ± 5%. We use NC film thickness ranging from 400 μm to 1700 μm and NC density ranging from 3.04 to 140 nanomoles per 1 mL of resin.

Nanocrystal photoluminescence color	**Crystal diameter (nm)**	**Peak emission wavelength (λ_{PL}) (nm)**
Cyan	1.9	500
Green	2.4	540
Yellow	3.2	580
Red	5.2	620

Table 5.1.3.1. Size of our nanocrystals.

Our cyan, green, yellow and red NCs exhibit photoluminescence (PL) peaks at 500 nm, 540 nm, 580 nm, and 620 nm, respectively, as characterized in Figure 5.1.3.1.

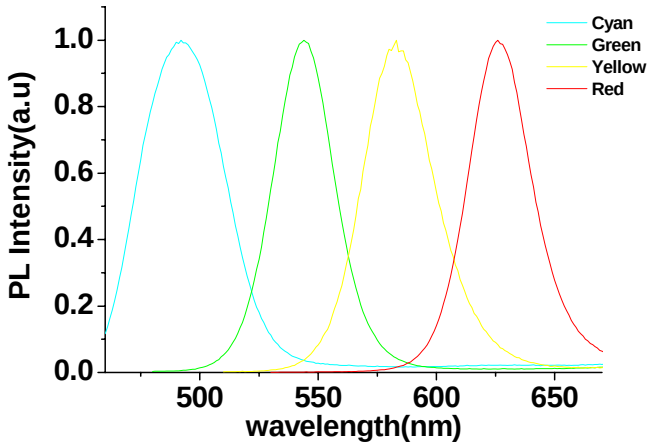

Figure 5.1.3.1. Photoluminescence spectra of our CdSe-ZnS core-shell nanocrystals in UV-curable resin.

5.1.4. Design, growth, fabrication and characterization of blue InGaN/GaN light emitting diodes

We use two types of blue InGaN/GaN LEDs, one with a peak electroluminescence at 440 nm and the other at 452 nm. We use an epitaxial layer design identical for both of the blue LEDs with the only change of the epitaxial growth temperatures of their respective active layers. The design of these InGaN/GaN LEDs is presented along with the thickness of each epitaxial layer in Figure 5.1.4.1.

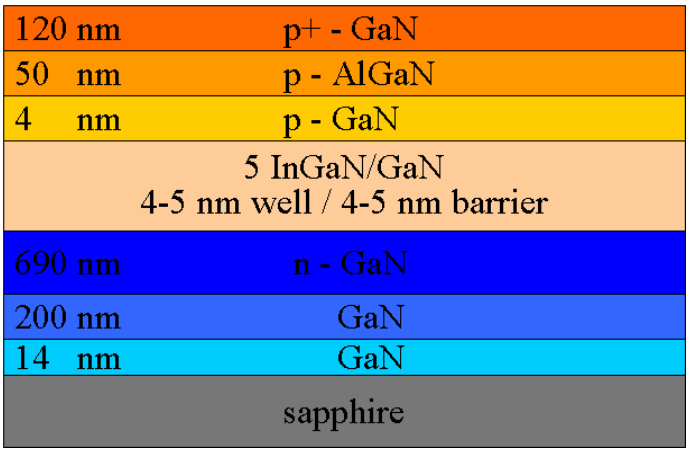

Figure 5.1.4.1. Epitaxial structure of our blue LEDs (not drawn to scale).

We use a GaN dedicated metal organic chemical vapor deposition (MOCVD) system (Aixtron RF200/4 RF-S) for the growth of our epitaxial layers at Bilkent University Nanotechnology Research Center. We start with a 14 nm thick GaN nucleation layer and a 200 nm thick GaN buffer layer to increase the crystal quality of the device epitaxial layers. Subsequently, we grow a 690 nm thick, Si doped n-type contact layer. We then continue with the epi-growth of five 4-5 nm thick InGaN wells and GaN barriers as the active layers of our LEDs. The growth temperature of this active region determines the amount of In incorporation into the wells, which in turn adjusts the emission peak wavelength. Therefore, we use distinct active region growth temperatures for the two types of our LEDs: one at 682°C for 440 nm EL peak and the other at 661°C for 452 nm EL peak. Finally, we finish our growth with p-type layers that consist of Mg-doped, 50 nm thick $Al_{0.1}Ga_{0.9}N$ and 120 nm thick GaN layers as the contact cap. Following the growth, we activate Mg dopants at 750°C for 15 minutes.

In the device fabrication, we use standard semiconductor processing including photolithography, thermal evaporator (metallization), reactive ion etch (RIE), and rapid thermal annealing. Our p-contacts consist of Ni/Au (15 nm/100 nm) and are annealed at 700^{o}C for 30 seconds under N_2 purge. On the other hand, our n-contacts consist of Ti/Al (100 nm/2500 nm) and are annealed at 600^{o}C for 1 minute under N_2 purge. The top-view micrographs of two of our fabricated blue LEDs (with λ_{EL}=440 nm in (a) and λ_{EL}=452 nm in (b)) are shown in Figure 5.1.4.2. For on-chip integration, following the surface treatment, we hybridize the LED top surface with various types of NCs in a UV curable host polymer. We cure the coated samples for one hour under the UV lamp for each film.

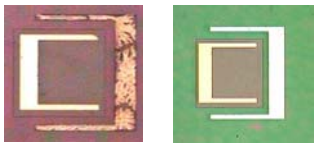

(a) **(b)**

Figure 5.1.4.2. Micrographs of our fabricated blue LEDs: (a) with λ_{EL}=440 nm and (b) with λ_{EL}=452 nm.

Our blue LEDs have turn-on voltages approximately at 4 V, and electroluminescence (EL) peak wavelengths at 440 nm and 452 nm, as shown in Figure 5.1.4.3.

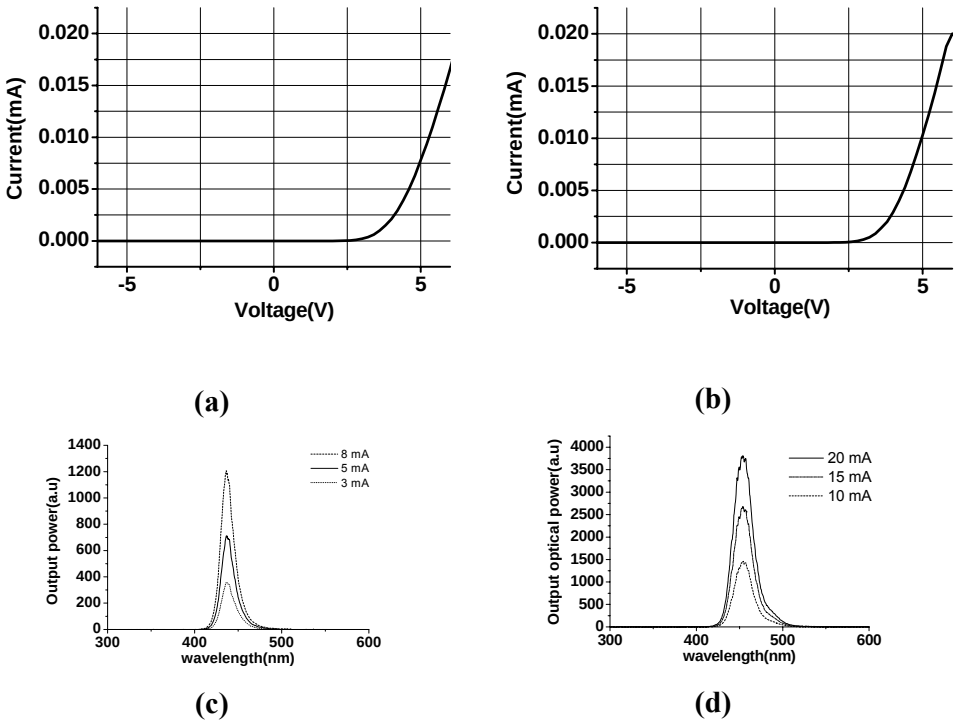

Figure 5.1.4.3. IV characteristics and electroluminescence spectra (at various current injection levels) of the LEDs with emission at 440 nm and 452 nm: IVs in (a) and (b), and ELs in (c) and (d), respectively.

5.1.5. Hybridizing single combination of CdSe/ZnS core-shell NCs with blue InGaN/GaN LEDs

Integrating our blue 440 nm InGaN/GaN LED with single yellow CdSe/ZnS core-shell NCs (with λ_{PL}=580 nm), we obtain electroluminescence spectra for different levels of current injection at room temperature, shown in Figure 6 along with a picture of the generated white light. Here to satisfy white light condition, we choose yellow NC for the hybridization on the blue LED and then design and realize the hybrid NC-LED with its NC film parameters set in accordance with our choice of NCs. Consequently, the emission spectra of the resulting hybrid NC-LED experimentally yield tristimulus coordinates of x=0.37

and y=0.25, a correlated color temperature of T_c=2692 K, and a color rendering index of R_a=14.6. This operating point mathematically falls within the white region of the C.I.E. (1931) chromaticity diagram. However, in this case, the resulting color rendering index is low as expected due to the dichromaticity of the hybridization of the yellow NC and the blue LED. Figure 5.1.5.1 also shows the location of the corresponding operating point on the (x,y) coordinates.

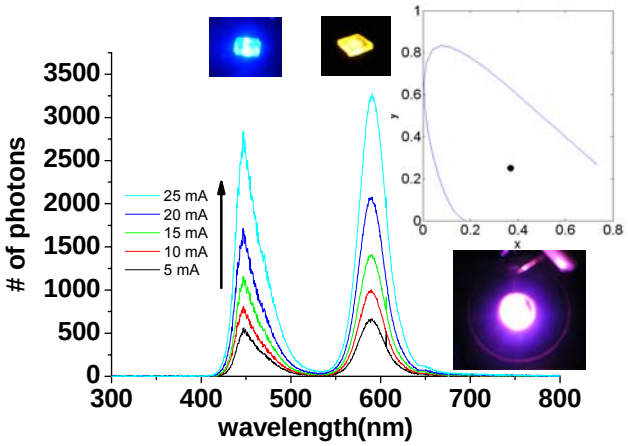

Figure 5.1.5.1. Electroluminescence spectra of yellow NC (λ_{PL}=580 nm) hybridized on blue LED (λ_{EL}=440 nm) at different levels of current injection at room temperature, along with the corresponding (x, y) coordinates and the pictures of the blue LED, yellow NC film, and hybrid NC-WLED while generating white light.

5.1.6. Hybridizing dual combination of CdSe/ZnS core-shell NCs with blue InGaN/GaN LEDs

Rather than a single type of NC, when we integrate our blue LED (λ_{EL}=440 nm) with a dual combination of cyan and red CdSe/ZnS NCs (λ_{PL}=500 nm and 620 nm, respectively) with the right device parameters, we obtain electroluminescence spectra at various injection currents at room temperature shown in Figure 5.1.6.1. Here we choose the combination of cyan and red NCs

so that their contributing photoluminescence mathematically satisfies the white light condition together with the electroluminescence of the integrating LED underneath them. In implementation, we place the red NC layer on the LED and the subsequent cyan NC layer on the red NC layer to minimize reabsorption of the photons emitted from the first NC layer when going through the second adjacent NC layer. In this case, the emission spectra leads to the operating point of x=0.37 and y=0.28, with T_c=3246 K and R_a=19.6. This is also located within the white region of the C.I.E chromaticity diagram, with the corresponding coordinates plotted in Figure 5.1.6.1. Here we observe that the color rendering index is improved using different NC types and covering larger ranges of the visible spectrum that contribute to white light.

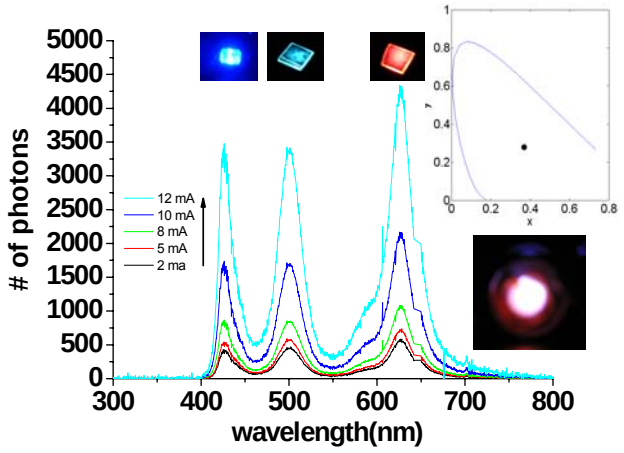

Figure 5.1.6.1. Electroluminescence spectra of a dual combination of cyan (λ_{PL}=500 nm) and red (λ_{PL}=500 nm) NCs hybridized with blue LED (λ_{EL}=440 nm) at various injection current levels at room temperature, along with (x, y) coordinates and the pictures of the LED, NC films and hybrid NC-WLED while generating white light.

5.1.7. Hybridizing trio combination of CdSe/ZnS core-shell NCs with blue InGaN/GaN LEDs

Hybridizing a trio combination of green, yellow, and red CdSe/ZnS NCs (λ_{PL}=540 nm, 580 nm, and 620 nm, respectively) on our 452 nm blue InGaN/GaN LED, we obtain electroluminescence spectra presented in Figure 5.1.7.1. In this design, we carefully choose the combination of green, yellow, and red NCs with the right hybridization parameters to satisfy the white light condition and place these NC films one after the other in the order of longer to shorter PL wavelength to prevent the reabsorption of emitted photons from each NC layer going through the subsequent NC layers. This implementation experimentally leads to x=0.30 and y=0.28 with T_c=7521 K and R_a=40.9, again falling within the white region of the C.I.E. chromaticity diagram shown in Figure 5.1.7.1. Here using a trio combination of NCs, the color rendering index is further improved.

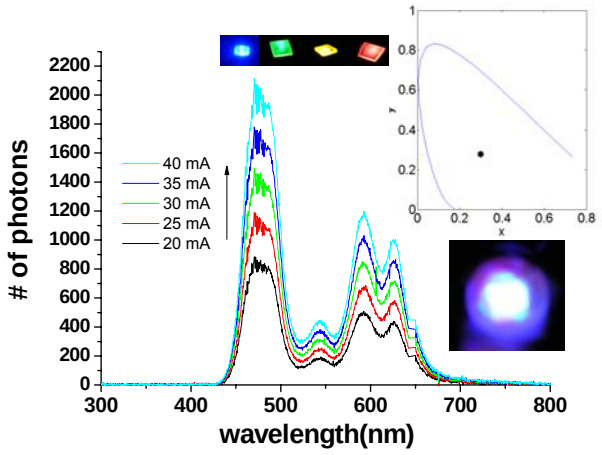

Figure 5.1.7.1. Electroluminescence spectra of a trio combination of green (λ_{PL}=540 nm), yellow (λ_{PL}=580 nm) and red (λ_{PL}=620nm) NCs with blue LED (λ_{EL}=452 nm) at various currents at room temperature, with (x, y) coordinates and the pictures of the LED, NC films and hybrid NC-WLED while generating white light.

5.1.8. Hybridizing quadruple combination of CdSe/ZnS core-shell NCs of with blue InGaN/GaN LEDs

Combining a quadruple combination of green (λ_{PL}=540 nm), cyan (λ_{PL}=500 nm), yellow (λ_{PL}=580 nm), and red (λ_{PL}= 620nm) NCs with the blue LED (λ_{EL}=452 nm), we obtain electroluminescence spectra corresponding to x=0.24 and y=0.33, with T_c=11171 K and R_a =71.0. This operating point falls in the white region of the C.I.E. chromaticity diagram like those of the previous hybrid NC-WLED. This time, however, the color rendering index is significantly improved due to the multi-chromaticity of this hybridization based on the combination choice of green, cyan, yellow, and red nanocrystals, while maintaining the white light condition. Here the combinations of our nanocrystals limit the maximum achievable color rendering index in our case, although it is possible to obtain a color rendering index higher than 90 using the right quadruple combination of nanocrystals in principle. Figure 5.1.8.1 shows the emission spectra at various injection current levels at room temperature, along with the picture of the generated white light.

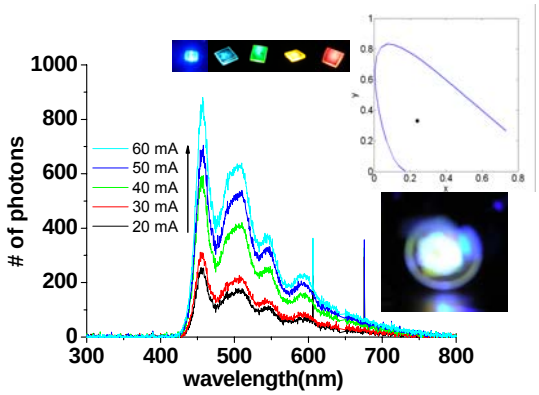

Figure 5.1.8.1. Electroluminescence spectra of quadruple combination of green (λ_{PL}=540 nm), cyan (λ_{PL}=500 nm), yellow (λ_{PL}=580 nm) and red (λ_{PL}= 620nm) NCs with blue LED (λ_{EL}= 452 nm) at various currents at room temperature, along with (x, y) coordinates and the pictures of the LED, NC films, and hybrid NC-WLED while generating white light.

5.1.9 Summary of characterisitics of hybrid white light emitting diodes

Hybridizing CdSe/ZnS core-shell NCs of various single, dual, trio, and quadruple combinations on our InGaN/GaN based blue LEDs, we demonstrate that the optical properties of the generated white light such as the tristimulus coordinates, color temperature, and color rending index are adjusted.

Using different NC types in the hybridization with the right hybrid device parameters, the color-rendering index is improved from 14.6 to 71.0. Table 5.1.9.1 provides a list of these hybrid NC-WLEDs, along with the corresponding (x, y) coordinates, color temperature, and color rendering index. Figure 5.1.9.1 depicts the operating (x, y) coordinates of these four hybrid NC-WLEDs that all fall in the white region of the C.I.E. chromaticity diagram.

LED λ_{EL}(nm)	NC λ_{PL} (nm)	(x,y)	T_c (K)	R_a
440	580	(0.37,0.25)	2692	14.6
440	500,620	(0.37,0.28)	3246	19.6
452	540, 580, 620	(0.3,0.28)	7521	40.9
452	540, 500, 580, 620	(0.24,0.33)	11171	71.0

Table 5.1.9.1. Our hybrid NC-WLED sample characteristics.

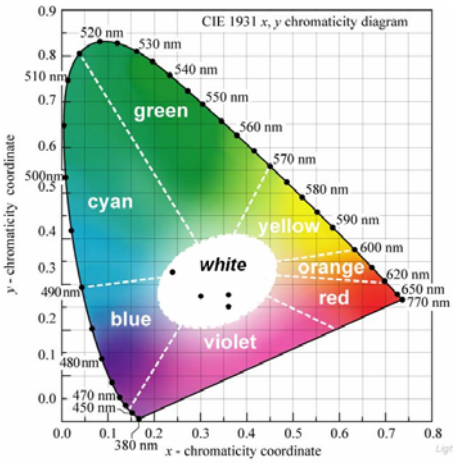

Figure 5.1.9.1. CIE 1931 (x, y) coordinates of our white hybrid NC-WLEDs.

5.2 Hybrid white light sources based on layer-by-layer assembly of nanocrystals on n-UV emitting diodes

In this part, we present the design, growth, fabrication, integration, and characterization of alternative hybrid white light sources based on the controlled layer-by-layer assembly of nanocrystals on UV-emitting nitride diodes for adjustable white light parameters. The first device includes layer-by-layer assembly of dichromatic cyan- and red-emitting nanocrystals (λ_{PL}=504-615 nm)

leading to the tristimulus coordinates (x=0.37,y=0.46); the second device uses the trichromatic combination of layer-by-layer hybridized cyan-, yellow-, and red-emitting nanocrystals (λ_{PL}=504-580-615nm) yielding (x=0.38,y=0.48). Such layer-by-layer hybridization offers advantages of precisely controlling individual nanocrystal film thicknesses and order in addition to concentrations. By utilizing such multiple combinations of nanocrystals in the assembly, the light parameters are well controlled and adjusted. To Leverage rapidly advancing UV technology into efficient lighting with nanocrystal based color conversion, it is critical to develop and demonstrate such hybrid light sources on UV pumping platforms.

5.2.1. Why n-UV LED platfrom rather than blue?

In hybrid NC-WLEDs, nanocrystal efficiency and hybridization significantly affect the device performance. In the previous section, blue LED platforms are used as the excitation sources as well as in the literature [23,24,26,27]. However, ultraviolet (UV) emitting LEDs provide a better platform for nanocrystal based white light generation for a number of reasons. First, at UV wavelengths, the absorption of nanocrystals is higher than in blue and, as a result, with UV pumping, thinner nanocrystal films are needed to achieve white light generation compared to blue pumping. Second, with a UV pump source, the white light emission results solely from the photoemission of the nanocrystals. This implies that the generated white light does not directly depend on the LED platform but only the combination of NC emitters, facilitating easier color tuning. Third, in the near future UV LEDs are expected to reach significantly higher optical power levels as increasingly aggressively

pushed forward by other industrial, wide-scale, high-power applications (e.g., photolithography, inkjet printing, resin curing, etc.). For this, the famous Japanese LED maker Nichia (where blue LEDs were invented [22]) has announced the production of UV LEDs with output optical powers up to 5 W in short term [28].

5.2.2 Hybridization of nanocrystal film on LED platform

For white light generation, we use CdSe/ZnS core-shell nanocrystals of crystal sizes 1.9 nm, 3.2 nm, and 5.2 nm (with a size distribution of ± 5%) from Evident. The emission colors of these nanocrystals are cyan, yellow, and red, tuned using the quantum size effect across the visible spectral range with their corresponding photoluminescence (PL) peaks at 504 nm, 580 nm, and 615 nm, respectively. These nanocrystals have high PL quantum yields ranging between 30-50%. Such core-shell NCs are shown to yield even higher efficiencies up to 66% [29]. We used similar type of nanocrystals also in our previous work for white light sources integrated on blue nitride LEDs [26,27] and nanocrystal based UV scintillators integrated on Si detectors [30]. In this work, we prepare high-concentration NC solutions to vortex-mix into host polymer of poly-methyl-methacrylate (PMMA). We evaporate NC films in micro-droplets of 25µl by drop-casting at 70-100^{o}C for optimal film formation and complete the polymerization process for each layer in the assembly. Figure 5.2.2.1 shows the photoluminescence and absorption spectra of our CdSe/ZnS core-shell nanocrystals in thin films of host PMMA.

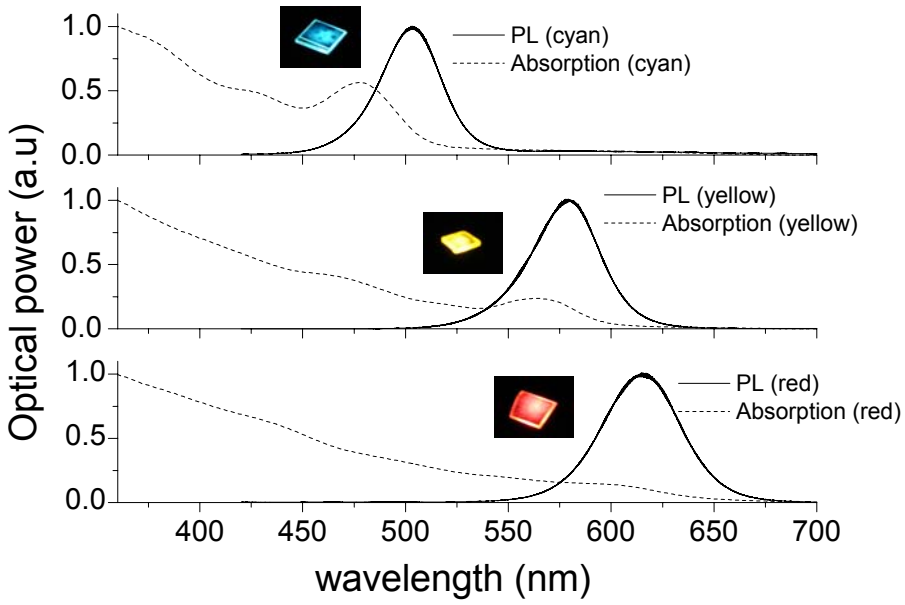

Figure 5.2.2.1. Photoluminescence (PL) and absorption spectra of our CdSe/ZnS core-shell nanocrystals in thin films at room temperature.

In this work, the hybrid light sources require much thinner NC films (hundreds of nanometers thick) in the case of UV pumping than the NC films (tens of micrometers thick) required for blue pumping in our previous work. Using ordered layers of such thin nanocrystal films, higher color rendering indices are obtained with UV pumping when compared to the results of dual and triple NC combinations used with blue pumping in our previous work.

5.2.3 Design, growth, fabrication and characterization of n-UV InGaN/GaN LED

We use InGaN/GaN based LEDs with a peak wavelength of 383 nm in the near ultraviolet as the pump source for the entire hybrid devices presented in this

subchapter. Figure 5.2.3.1 shows the design of our LEDs. For the epitaxial growth, we use a GaN dedicated metal organic chemical vapor deposition (MOCVD) system. First, we begin with a 14 nm thick GaN nucleation layer. To increase the crystal quality of the subsequent epitaxial layers, we then grow a 200 nm thick GaN buffer layer. For the n-type contact, we grow a 690 nm thick, Si doped epitaxial layer. For the active layers, we continue the epi-growth with five 2-3 nm thick InGaN wells and GaN barriers at a growth temperature of 720°C. We finish our growth with the p-type layers that consist of a 50 nm thick Mg-doped AlGaN layer and a 120 nm thick Mg-doped GaN layer as the contact cap. Finally, we activate the Mg dopants at 750°C for 15 minutes. We used similar growth steps for the development of our GaN based quantum electroabsorption modulators [31].

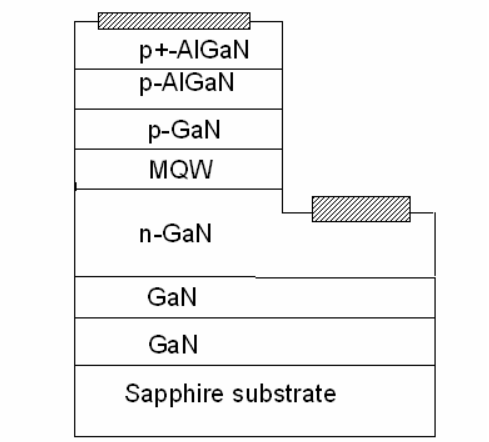

Figure 5.2.3.1. Epitaxial structure of our n-UV LED.

Our device fabrication follows standard semiconductor processing procedures as in our previous work [31-33]. These include photolithography, thermal

evaporation (metallization), reactive ion etch (RIE), and rapid thermal annealing. We use photolithography and reactive ion etching (down to 940 nm) to expose the n-type layer and then apply thermal evaporation to deposit the metal contacts. We form the ohmic p-contacts with the metal deposition of 15 nm of Ni with a 100 nm overlayer of Au followed by rapid thermal annealing at 700°C for 30 s. We lay down a 10 nm layer of Ti with a 200 nm overlayer of Al for the n-contacts followed by a rapid thermal anneal at 600°C for 1 minute under nitrogen.

Figure 5.2.3.2 (a) shows the IV characteristics of our fabricated n-UV LEDs with turn-on voltages at approximately 5 V and Figure 5.2.3.2 (b) shows their electroluminescence (EL) spectra under different levels of current injection, with the EL peak wavelength at 383 nm. In hybrid devices, this high-energy electroluminescence of the LED excites the integrated NC layers, resulting in spontaneous emission from each NC layer. In hybrid devices, the electrically driven UV LED optically pumps the NCs and the photoluminescence of these NC layers then collectively generates the white light. However, when blue LED is used as the excitation source, the LED platform additionally contributes directly to the white light generation.

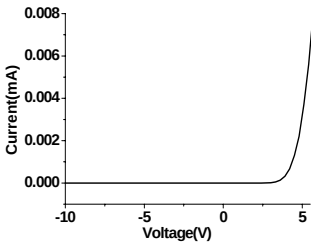

(a)

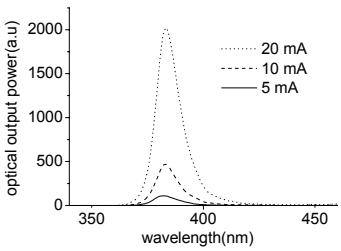

(b)

Figure 5.2.3.2. (a) IV and (b) electroluminescence (EL) spectra (λ_{EL}=383 nm) of our n-UV LEDs under different levels of current injection at room temperature.

5.2.5 Dichromic combination of nanocrystals on n-UV InGaN/GaN LED

For the dichromatic combination, we employ cyan and red NCs (λ_{PL}=504 nm and 615 nm). At first we integrate 650 nm thick cyan-emitting NC film with a 23% volume ratio of the NCs to the host PMMA. On top of this layer, we hybridize 575 nm thick red-emitting NC film with a 13% volume ratio. In our previous work, much thicker NC films were required for blue pumping [26,27]. Figure 5.2.5.1 demonstrates the electroluminescence spectra of this n-UV LED hybridized with dichromatic nanocrystal combination at various current injection levels. The resulting tristimulus coordinates are (x, y)=(0.37, 0.46) in the near-white region. The correlated color temperature and color rending index are T_c=4520 K and R_a=43.1. Such operating points were also previously obtained using blue LED pumps, e.g., in [26,27]. Because of the dichromaticity, the color rendering index is low here. To improve the white light quality, we work with triple combinations of NCs next.

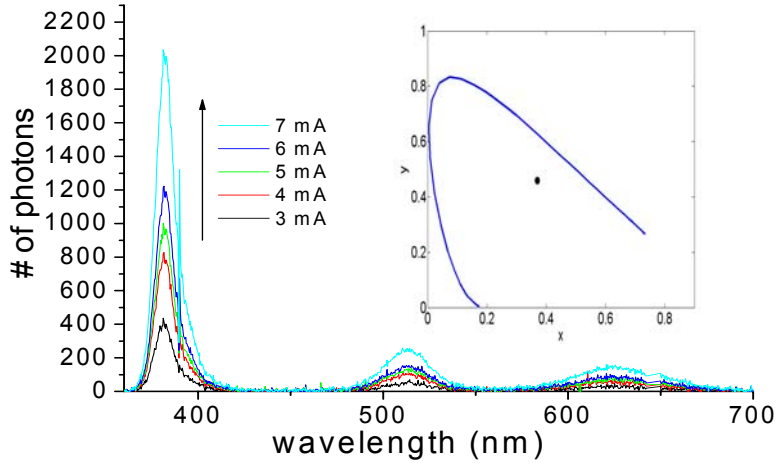

Figure 5.2.5.1. Electroluminescence spectra of dichromatic combinations of cyan (λ_{PL}=504 nm) and red (λ_{PL}=615 nm) nanocrystals hybridized on an n-UV LED for various current levels at room temperature.

5.2.6 Trichromic combination of nanocrystals on n-UV InGaN/GaN LED

For hybridizing trichromatic combinations of NCs, we use cyan, yellow, and red NCs (λ_{PL}=504 nm, 580 nm, and 615 nm) on an n-UV LED. We integrate NC films of 650 nm in thickness each with a 23% NC-to-host volume ratio in the assembly, in the order of cyan, yellow, and red from bottom to top. Figure 5.2.6.1 shows the electroluminescence spectra of integrated white LEDs with triple NC combinations at various current injection levels. These spectra correspond to x=0.38, y=0.48, T_c= 4434 K, and R_a= 67.6. In this case, the color rendering index is significantly improved compared to the dichromatic combination. Here it is worth noting that these WLEDs, which consist of the dual and triple NC combinations pumped by n-UV excitation LEDs, are improved in terms of color rendering indices also when compared to our previous work using blue LED pumps [26,27]. The CdSe/ZnS NCs available at

our labs cover the visible spectrum from cyan (504 nm) to red (615 nm); their possible combinations are thus confined within the shaded region (color gamut) of the color chromaticity diagram shown in Figure 5.2.6.2. One future direction of our research work is to expand this color gamut to include the center of white region (~0.33, ~0.33) using nanocrystals emitting at <490 nm to further improve the white light quality. Table 5.2.6.1 presents a summary of the optical characteristics of our hybrid NC-LED sources [36,37].

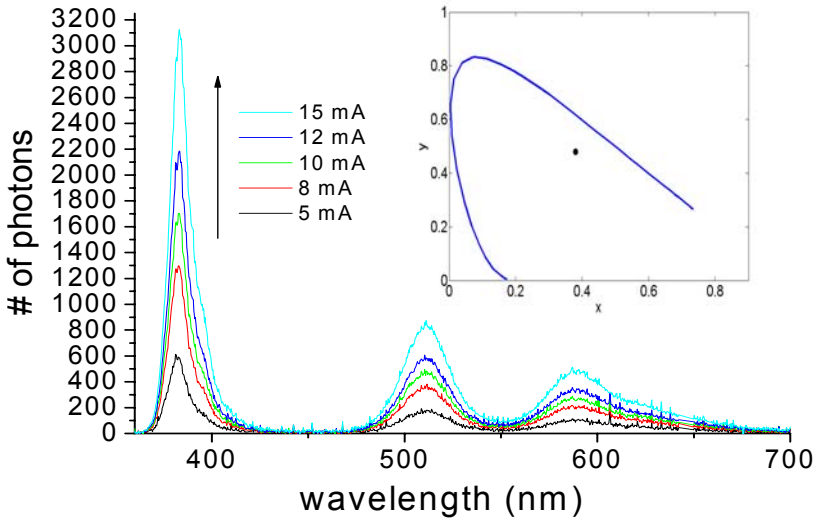

Figure 5.2.6.1. Electroluminescence spectra of trichromatic combinations of cyan (λ_{PL}=504 nm), yellow (λ_{PL}=580 nm), and red (λ_{PL}=615 nm) emitting nanocrystals hybridized on an n-UV LED for various current levels at room temperature using UV LED pump.

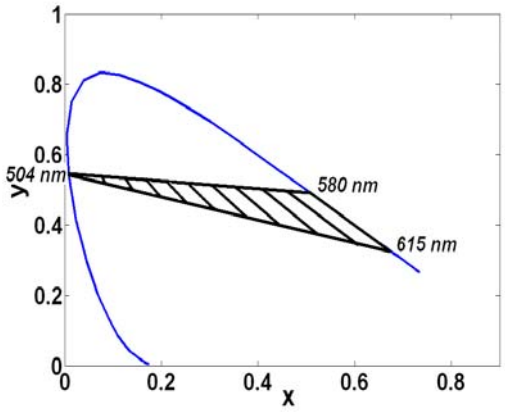

Figure 5.2.6.2. Color gamut covered using cyan, yellow and red CdSe/ZnS nanocrystals in the C.I.E. color chromaticity diagram.

Nanocrystal combination	X	y	T_c (K)	R_a
Double (cyan and red)	0.37	0.46	4529	43.1
Triple (cyan, yellow, and red)	0.38	0.48	4434	67.6

Table 5.2.6.1. Summary of the optical characteristics of our hybrid NC-LED sources.

5.3 Nanocrystal based white light generation with tunable color parameters by using blue and n-UV InGaN/GaN light emitting diodes

In this part, in 26 of our NC-LED samples, we experimentally show the effect of the NC concentration and NC film thickness on tuning the color properties of the generated light (tristimulus coordinates, color rendering index, and correlated temperature) [36,37], as shown on the C.I.E. chromacity diagram in Figure 5.3.1. We further compare layer-by-layer assembly and blending of NCs for integration on LEDs. Using combinations of nanocrystals and organizing

them mixed and/or unmixed in layers, we tune the color parameters of the generated light.

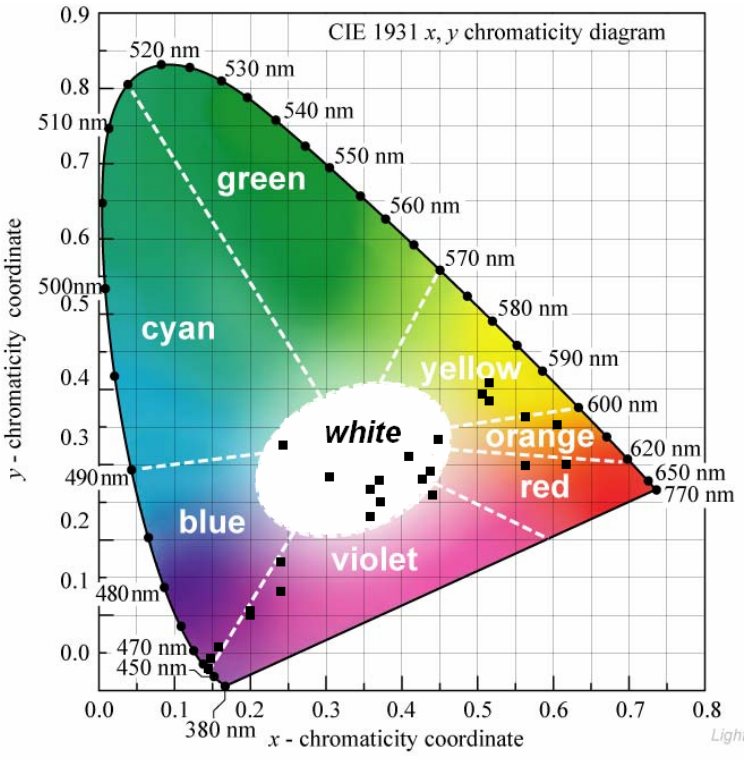

Figure 5.3.1. Tristimulus coordinates of our hybrid NC-WLEDs on the C.I.E. (1931) chromaticity diagram

For this work, we use blue and n-UV InGaN/GaN light emitting diodes and nanocrystals from Evident Technologies that are explained in previousSections 5.1 and 5.2. Table 5.3.1 lists 26 different samples of our hybrid light sources along with their corresponding tristimulus coordinates, correlated color temperature, and color rendering index.

Sample #	Hybridized nanocrystals	LED λ_{EL} (nm)	Concentration (μmol/mL)	x	y	T_c (K)	R_a
1	-	452	-	0.14	0.03	34367	-51.5
2	Y	452	2.36	0.15	0.04	34367	-40.2
3	Y	452	2.36	0.16	0.06	34367	-28.6
4	Y	452	2.36	0.20	0.10	34366	-10.1
5	Y	452	2.36	0.24	0.13	34366	-3.8
6	Y	452	2.36	0.43	0.28	1882	15.8
7	G,Y	452	5.59, 2.36	0.44	0.29	1989	37.5
8	G,Y	452	5.59, 2.36	0.45	0.33	2165	54.5
9	G,Y	452	5.59, 2.36	0.52	0.37	1754	50.2
10	R,Y	452	0.88, 2.36	0.57	0.30	1121	42.2
11	R,Y	452	0.88, 2.36	0.62	0.30	1000	50.7
12	C,Y	452	12.05, 2.36	0.24	0.13	34366	-3.4
13	C,Y	452	12.05, 2.36	0.36	0.23	2651	32.4
14	C,Y	452	12.05, 2.36	0.36	0.27	3228	48.3
15	C,Y	452	12.05, 2.36	0.42	0.31	2311	50.2
16	Y	440	0.11	0.37	0.25	2692	14.6
17	C,Y	440	0.37, 0.11	0.37	0.28	3246	19.6
18	G,Y,R	452	0.27, 0.11, 0.025	0.30	0.28	7521	40.9
19	C,G,Y,R	452	0.37,0.27,0.1,0.025	0.24	0.33	11171	71.0
20*	C,Y,R	452	2.54, 0.19, 0.06	0.44	0.26	1625	38.8
21	C,Y,R	452	2.8,2.8, 2.8	0.20	0.10	34366	1.9
22	C,Y,R	383	2.8,2.8, 2.8	0.51	0.39	1979	71.9
23*	C,Y,R	383	2.54, 0.19, 0.06	0.61	0.36	1238	74.3
24	C,R	452	2.8,2.8	0.20	0.11	34367	4.0
25*	C,R	452	2.73,0.06	0.24	0.13	34366	-13.8
26*	C,R	383	2.73,0.06	0.57	0.37	1477	47.6
27	C,R	383	2.8,2.8	0.52	0.41	1977	42.1

Table 5.3.1. Our hybrid NC-WLED sample characteristics. (C: cyan NC; G: green NC; Y: yellow NC; R: red NC; * denotes blended NC hybridization.)

Sample 1 shows one of the blue LEDs with electroluminescence peak at 452 nm as the starting platform. For Samples 2-6, we hybridize yellow NCs on this blue LED. In Sample 2, we integrate 25 μl NCs in toluene with 3.1 μl PMMA solution corresponding to a concentration of 2.36 μmol/ml. For each subsequent sample (from Sample 2 to Sample 6), we increase the NC solution by multiples of 25 μl and PMMA by 3.1 μl. For Sample 6, we end up with 150 μl NCs solution and 18.75 μl PMMA corresponding to a final concentration of 2.36

μmol/ml. Consequently, on the C.I.E. chromaticity diagram, (x, y) tristimulus coordinates of these samples begin with (0.14, 0.03) on the blue edge for 452 nm and reaches (0.43, 0.28) in the white region. The correlated color temperature ranges from cool white colors to warm white colors as we increase the hybridized NCs solution. Furthermore, the color rendering index starts with -51.5, increases in each step and reaches 15.8 as a dichromatic source. Therefore, we observe experimentally that the thickness of the hybridized NC thin films significantly shift the color parameters of the resulting hybrid LEDs. Figure 5.3.2 shows the optical spectrum of Sample 6 to observe the increase in yellow peak with respect to electroluminescence of blue LED.

For Samples 7-9, we increase green NC volume in toluene by 25 μl and PMMA by 3.1 μl corresponding to a concentration of 5.59 μmol/ml and on top of the green NC film, we place 150 μl yellow NCs and 18.75 μl PMMA having a concentration of 2.36 μmol/ml. As a result, the tristimulus coordinates of these samples move from (0.44, 0.29) to (0.52, 0.37). The corresponding correlated color temperatures move towards warm white to 1754 K.

When 150 μl yellow NCs and 18.75 μl PMMA with a concentration of 2.36 μmol/ml are hybridized on the blue LED at 452 nm, the color rendering index is only 15.8 (due to the dichromacity of the source). However, when 75 μl green NC and 9.3 μl PMMA with a concentration of 5.59 μmol/ml and 150 μl yellow NC and 18.75 μl PMMA with a concentration of 2.36 μmol/ml are hybridized layer-by-layer in the respective order, the color rendering index becomes 50.7 (because of the trichromaticity of the source). Figure 5.3.3 shows the optical

spectrum of this hybrid LED (Sample 9). For Samples 10 and 11, we similarly observe increase in correlated color temperature and color rendering index by adding red NCs instead of green NCs.

For Samples 12-15, we hybridize cyan NC film first and then add 150 μl yellow NCs and 18.75 μl PMMA having a concentration of 2.36 μmol/ml on top of it. In each sample, we add 25 μl cyan NCs in toluene and 3.1 μl PMMA corresponding to an additional concentration of 12.05 μmol/ml. By increasing the incorporation of cyan NCs, the tristimulus coordinates move closer to the cyan part of the C.I.E. chromaticity diagram, which would imply the correlated color temperature to increase. However, on the contrary, in our samples we observe that the correlated color temperature of our hybrid NC-LEDs decrease and become a warmer light source. According to our observations, this behavior stems from the reabsorption of the photons generated by the cyan NCs in the top yellow NC film. Figure 5.3.4 shows the optical spectrum of 75 μl cyan and 9.3 μl PMMA corresponding to a concentration of 12.05 μmol/ml and 150 μl yellow NCs and 18.75 μl PMMA having a concentration of 2.36 μmol/ml hybridized on the blue LED with the peak electroluminescence of 452 nm. In Table 5.3.1, Samples 16-19 are also discussed in Section 5.1 [26,27].

For Samples 20-27, we incorporate NCs either blended in a mixture or assembled layer-by-layer. The samples indicated with * in Table 5.3.1 are those that are directly hybridized by blending all the NCs as a mixture and integrated on the LED (rather than placing layer-by-layer). To compare the optical properties of these two cases, we select Sample 20 and Sample 21. Sample 20

consists of blended cyan, yellow, and red NCs. On the other hand, for Sample 21, we integrate first the red NC film, on top of which comes the yellow NC film and then finally cyan NC film to prevent the reabsorbtion of the generated photon by the subsequent films. For each sample, the number of NCs per unit volume (NC concentration) is approximately constant. Figure 5.3.5 shows the optical spectrum of both Samples 20 and 21. Although the red peak is higher in Sample 20, its cyan peak is lower compared to Sample 21. This is because the photoluminescence of the cyan NCs has the probability to be reabsorbed by the red and yellow NCs, which reduces the cyan peak in the blended case in Sample 20. Additionally, red and yellow NCs can be further pumped also by the photon emitted from the cyan NCs, increasing the red peak. However, in layer-by-layer assembly in Sample 21, since the cyan NC film is on the top, there is no probability of reabsorption of photoluminescence of cyan NCs.

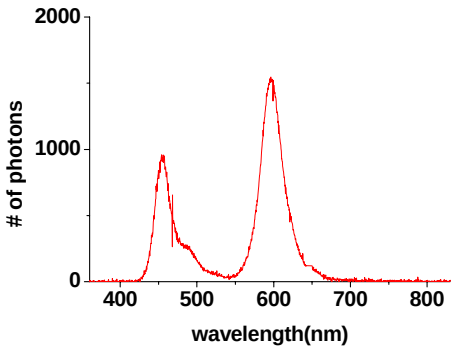

Figure 5.3.2. Electroluminescence spectrum of 150 µl yellow NCs (λ_{PL}=580 nm) and 18.75 µl PMMA corresponding to a film concentration of 12.05 µmol/mL hybridized on blue LED (λ_{EL}=452 nm) measured at an injection current level of 5 mA at room temperature.

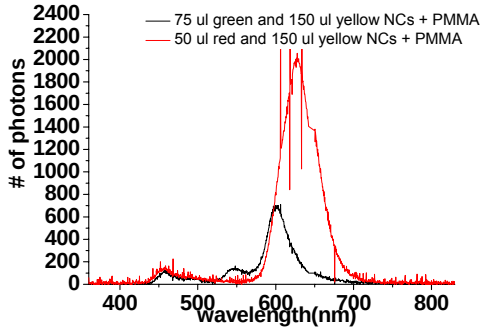

Figure 5.3.3. Electroluminescence spectrum of 75 µl green NC and 9.3 µl PMMA corresponding to a film concentration of 5.59 µmol/mL and 150 µl yellow NCs (λ_{PL}=540 nm and 580 nm) and 18.75 µl PMMA corresponding to a film concentration of 12.05 µmol/mL hybridized with blue LED (λ_{EL}=452 nm) at an injection current level of 5 mA and the electroluminescence spectrum of 50 µl red NC and 6.2 µl PMMA corresponding to a film concentration of 0.88 µmol/mL and 150 µl yellow NCs (λ_{PL}=620 nm and 580 nm) and 18.75 µl PMMA corresponding to a film concentration of 12.05 µmol/mL hybridized on blue LED (λ_{EL}=452 nm) measured at an injection current level of 5 mA at room temperature.

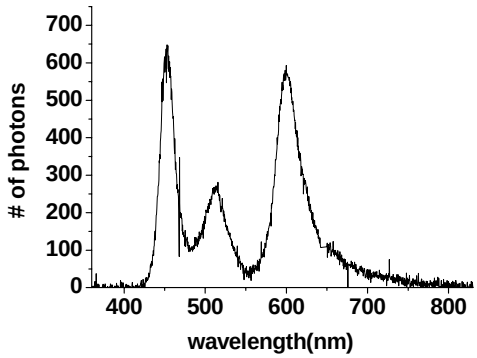

Figure 5.3.4. Electroluminescence spectrum of 75 µl cyan NC and 9.3 µl PMMA corresponding to a film concentration of 12.05 µmol/mL and 150 µl yellow NCs (λ_{PL}=500 and 580 nm) and 18.75 µl PMMA corresponding to a film concentration of 12.05 µmol/mL hybridized on blue LED (λ_{EL}=452 nm) measured at an injection current level of 5 mA at room temperature.

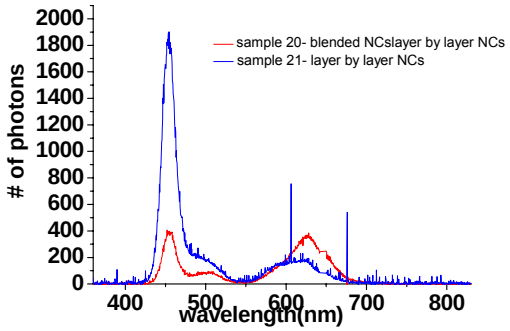

Figure 5.3.5. Electroluminescence spectra of samples 20 and 21. Sample 20 consists of blended mixture of 75 µl cyan NC, 25 µl yellow NC, and 25 µl red NC (λ_{PL}=540 nm, 580 nm and 620 nm) and 2 µl, 6 µl and 80 µl PMMA mixtures respectively, corresponding to film concentrations of 2.54 µmol/ml, 0.19 µmol/ml, and 0.06 µmol/ml. Sample 21 consists of layer-by-layer hybridization of 75 µl cyan NC, 25 µl yellow NC, and 25 µl red NC (λ_{PL}=540 nm, 580 nm and 620 nm) and 88 µl PMMA, corresponding to a film concentration of 2.8 µmol/mL, respectively.

5.4. White light generation tuned by dual hybridization of nanocrystals and conjugated polymers

Polymers and nanocrystals (NCs) with their promising optical properties are strong candidates for future lighting technology. White light generation utilizing different polymers have previously been investigated [11,38-56]. Among various polymer types, specifically conjugated polymers are promising candidates in lighting applications. They have very strong absorption both in n-UV and blue on the order of 10^5 cm^{-1} with very high quantum efficiency, which is better than phosphors. Additionally polymers can be deposited easily with common techniques such as dipping and spin coating and noticeably they are almost free from concentration quenching effects [11]. Similarly, nanocrystals have also recently been used for color conversion in white light generation.

They also show very promising properties including narrow emission spectra widely tunable across the visible spectral range, small overlap between their emission and absorption spectra, and the ability to easily and uniformly deposit their films with common techniques such as evaporation, spin casting, and dip coating.

In this thesis here, unlike in the previous research work, the combined use of conjugated polymers and NCs for white light generation on the same n-UV LED platform is shown. The white light generation by different combinations of polyfluorene and nanocrystals affording high color rendering indices is demonstrated; the tunability of the generated white light is studied. In this work, the combinations incorporated on our n-UV LEDs include ***1.)*** yellow nanocrystals (λ_{PL} = 580 nm) and blue polyfluorene (λ_{PL} = 439 nm) with tristimulus coordinates of *(x, y) = (*0.31*,* 0.27*)*, a correlated color temperature of T_c = 6962 K and a color rendering index of R_a = 53.4 shown in Figure 5.4.1 (a); ***2.)*** yellow and green nanocrystals (λ_{PL} = 580 and 540 nm) and blue polyfluorene (λ_{PL} = 439 nm) with *(x, y) = (*0.23*,* 0.30*)*, T_c = 14395 K and R_a = 65.7 shown in Figure 5.4.1 (b); and ***3.)*** yellow, green and red nanocrystals (λ_{PL} = 580, 540 and 620 nm) and blue polyfluorene (λ_{PL} = 439 nm) with *(x, y) = (*0.38*,* 0.39*)*, T_c = 4052 K and R_a = 83.0 shown in Figure 5.4.1 (c). Here, along with nanocyrstals emitting in red, yellow and green, the polyfluorene serves an important function of efficient emission in blue, for it is much more difficult to obtain high efficiency emission with nanocrystals at the shorter wavelengths (for example, in the blue). With such dual use of polyfluorene and nanocrystals, the color

rendering index is well controlled and significantly improved by increasing multi-chromaticity of the nanocrystal and polymer emitters. In so doing, high color rendering index (>80) exceeding the requirements of the future solid state lighting applications is achieved [57].

(a) **(b)** **(c)**

Figure 5.4.1. Image of white light emission from hybrid nanocrystal-conjugated polymer based white light emitting diodes: (a) yellow nanocrystals (λ_{PL} = 580 nm) and blue polyfluorene (λ_{PL} = 439 nm) (b) yellow and green nanocrystals (λ_{PL} = 580 and 540 nm) and blue polyfluorene (λ_{PL} = 439 nm) (c) yellow, green, and red nanocrystals (λ_{PL} = 580, 540 and 620 nm) and blue polyfluorene (λ_{PL} = 439 nm), and (d) blends of yellow, green, and red nanocrystals (λ_{PL} = 580, 540 and 620 nm) and blue polyfluorene (λ_{PL} = 439 nm) on a n-UV LED (λ_{EL} = 383 nm).

5.4.1 Properties of conjugated polymers and nanocrystals

The absorption maximum of conjugated polymer polyfluorene in $CHCl_3$ solution is $\lambda_{max,abs}$ = 382 nm, and the emission maximum is found to be λ_{PL} = 414 nm, as shown while photoemitting in blue in Figure 5.4.1.2 (a). In addition to the polyfluorene conjugated polymer, three types of nanocrystals are utilized as color-selectable emitters with tunable photoluminescence in the visible spectral range. Their emission colors are green, yellow, and red (shown in Figure 5.4.1.2 (b)-(d)), tuned using the quantum size effect across the visible with their corresponding photoluminescence peaks at 540 nm, 580 nm, and 615 nm, respectively. The photoluminescence of the polymer and NC emitters is

shown altogether in Figure 4. These nanocrystals available from Evident have high PL quantum yields ranging between 30-50%. Such core-shell NCs have been shown to yield even higher efficiencies up to 66% [29]. These nanocrystals have crystal diameters of 2.4 nm, 3.2 nm, and 5.2 nm and exhibit a size distribution of ± 5%. Their respective molecular weights are 14 μg/nmol, 38 μg/nmol, and 180 μg/nmol. Such types of nanocrystals have been used in our previous work for white light sources integrated on nitride LEDs [26, 34] and nanocrystal based UV scintillators integrated on Si detectors [30]. In this work, high concentration NC solutions are prepared and NC films are evaporated for optimal film formation. Here the hybrid device parameters including the type and film thickness of closely packed NC emitters, the concentration and film thickness of polymer emitters, and the order of NC and polymer films are controlled to adjust optical properties of the generated white light. These parameters affect the color conversion rate and thus the relative optical power of NC and polymer PL peaks contributing to the spectrum. By using different number of NC-polymer combinations as such, the intervals of the spectrum to contribute to the white light generation are set. By changing the order of NC and polymer films, the level of reabsorption of the photons emitted by the previous layers is adjusted. Increasing the number of combinations, multi-chromatic sources are achieved to generate white light with high color rendering indices. Such an ability to control these hybrid device parameters enables to tune the optical properties of the generated white light as desired.

Figure 5.4.1.1. (a) Photograph of polyfluorene photoluminescence in blue. (b) the green NC film, (c) the yellow NC film, and (d) the red NC film.

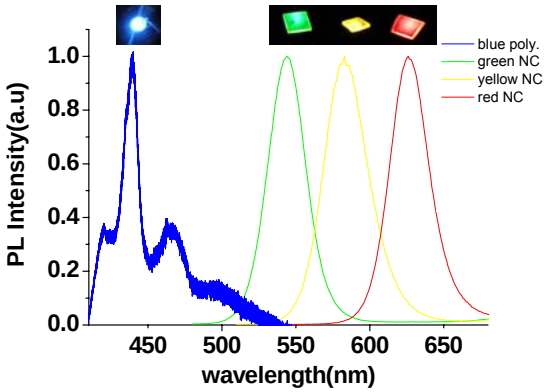

Figure 5.4.1.2. Photoluminescence spectra of the blue emitting conjugated polymer polyfluorene, and green, yellow, and red emitting CdSe/ZnS nanocrystals.

5.4.2 White light generation by polyfluoerene with single combination of nanocrystal

To obtain white light, our InGaN/GaN n-UV LED (λ_{EL} = 383 nm) that we explained in Chapter 5.2 is first integrated with blue emitting polyfluorene polymers (λ_{PL} = 439 nm) and single type yellow CdSe/ZnS core-shell nanocrystals (λ_{PL} = 580 nm) on the top. The hybridization parameters are carefully designed to satisfy white light condition with the highest possible color rendering index, considering the optical properties of the polyflourene, NC and LED. For that, a 135 nm thick layer of closely packed yellow NCs and a 1.06 μm thick layer of 3 mg/ml blue polymer are hybridized on to the LED. The electroluminescence spectra of the resulting hybrid polymer-NC LED are

obtained at different levels of current injection to the LED at room temperature as shown in Figure 5.4.2.1. These emission spectra experimentally yield tristimulus coordinates of x = 0.31 and y = 0.27, a correlated color temperature of T_c = 6962 K, and a color rendering index of R_a = 53.4. This operating point falls into the white region in the 1931 C.I.E. chromaticity diagram depicted in Figure 5.4.2.1. In our previous work, for such a dichromatic source where only yellow nanocrystals (λ_{PL} = 580 nm) were hybridized on a 440 nm blue InGaN/GaN LED, a color rendering index of at most 14.6 was acquired [26-27]. Here instead of blue LEDs, using blue polyfluorene, whose emission spectrum is broader, a higher color rendering index is achieved. However, given the requirements of future lighting, this color rendering index is yet not sufficient, which motivates further hybridization of other NCs on the hybrid device.

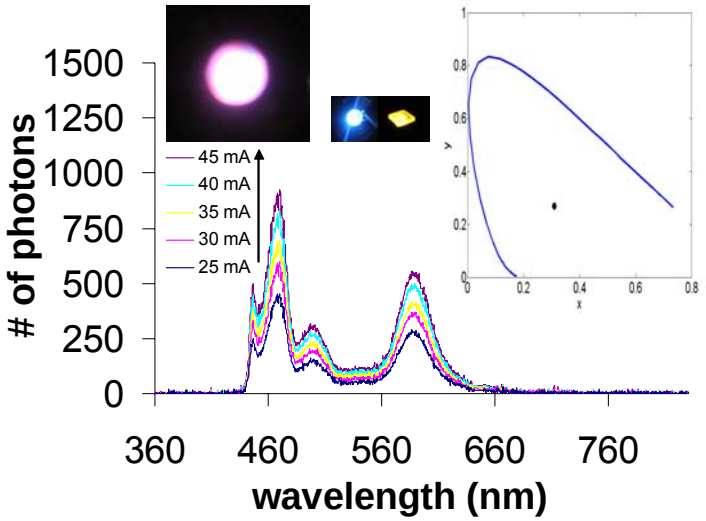

Figure 5.4.2.1. Electroluminescence spectra of yellow CdSe/ZnS core-shell nanocrystals (λ_{PL} = 580 nm) and blue polyfluorene conjugated polymer (λ_{PL} = 439 nm) deposited layer-by-layer on an InGaN/GaN n-UV LED (λ_{EL} = 383 nm) at different levels of current injection (room temperature). Pictures of the generated white light, blue emission of the polymer and yellow emission of the

nanocrystals are depicted. The location of the corresponding operating point on the *(x, y)* chromaticity coordinates is displayed.

5.4.3 White light generation by polyfluoerene with dual combination of nanocrystal

For the second set, instead of using single nanocrystal film, two types of green and yellow CdSe/ZnS core-shell nanocrystals (λ_{PL} = 540 and 580 nm) in combination with the blue emitting polyfluorene (λ_{PL} = 439 nm) are hybridized on our InGaN/GaN n-UV LED (λ_{EL} = 383 nm). For this combination, the right hybridization parameters are again carefully selected to increase the color rendering index while satisfying the white light condition. For that, a 1.06 μm thick film of 3 mg/ml blue polymer followed by a 400 nm thick film of closely packed green NCs and topped by a 70 nm thick film of closely packed yellow NCs are used. The electroluminescence spectra of the resulting hybrid device obtained at different levels of current injection at room temperature are shown in Figure 5.4.3.1. This implementation experimentally leads to tristimulus coordinates of x = 0.23 and y = 0.30, a correlated color temperature of T_c = 14395 K, and a color rendering index of R_a = 65.7, which again mathematically corresponds to the white region of the C.I.E. chromaticity diagram as desired. Here with the right design, a significant improvement in the color rendering index is achieved as the chromaticity is increased from dichromatic source to trichromatic source by the addition of green nanocrystals.

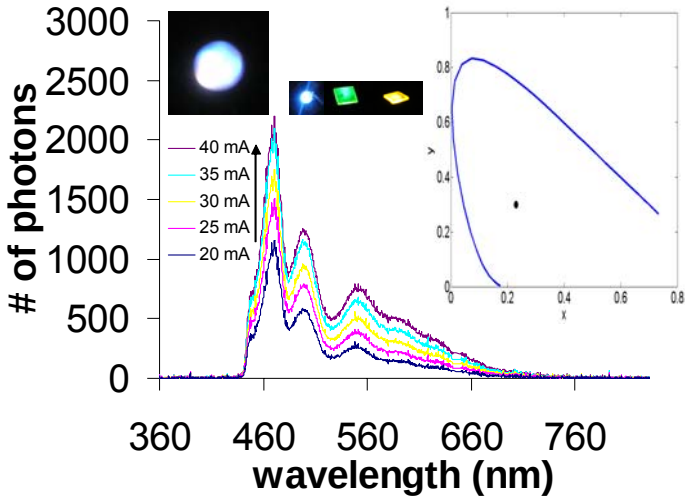

Figure 5.4.3.1. Electroluminescence spectra of blue polyfluorene (λ_{PL} = 439 nm) and green and yellow CdSe/ZnS core-shell nanocrystals (λ_{PL} = 540 and 580 nm) layer-by-layer hybridized on an InGaN/GaN n-UV LED (λ_{EL} = 383 nm) at different levels of current injection (at room temperature) along with a picture of the generated white light (blue polymer and green and yellow nanocrystals); and the location of the corresponding operating point on the *(x, y)* coordinates.

5.4.4 White light generation by polyfluoerene with trio combination of nanocrystal

For the third set, rather than using dual nanocrystal combination, three types of nanocrystals (yellow, green, and red at λ_{PL} = 580, 540, and 620 nm, respectively) are integrated with blue polyfluorene (λ_{PL} = 439 nm) on our InGaN/GaN n-UV LED (λ_{EL} = 383 nm). Again, the hybrid device is carefully designed for increased white light quality. The color properties of the resulting hybrid LED are monitored step by step after hybridization of each emitter layer. First, a 1.03 μm thick layer of 3 mg/ml blue polymer is hybridized on top of the n-UV LED (named CRI Test Sample 1 here). In this case, the resulting electroluminescence corresponds to tristimulus coordinates of x = 0.18 and y = 0.21, a correlated

color temperature of T_c = 34463 K, and a color rendering index of R_a = 49.5. After further integrating an approximately 400 nm thick film of closely packed green NCs on top of the polymer, the optical properties are shifted to x = 0.32 and y = 0.37 to fall into the white region with R_a = 66.0 and T_c = 5896 K (named CRI Test Sample 2). With this additional emitter layer, the color rendering index increases approximately by 16 units and the color temperature decreases by 28567 K moving towards the planckian sources on the red side. Subsequently, the device is further hybridized with a 135 nm thick film of closely packed yellow NCs, yielding x = 0.32, y = 0.37, T_c = 5694 K, and R_a = 73.7 (named CRI Test Sample 3). Here the color rendering index further increases to 73.7 and the correlated color temperature further decreases to 5694 K. Finally, a 292 nm thick layer of closely packed red NCs is integrated on the very top. Consequently, this leads to an improved color rendering index of R_a = 83.0 and a decreased correlated color temperature of T_c = 4052 K at the operating point of x = 0.38, y = 0.39 (named CRI Test Sample 4). In Figure 5.4.4.1, the electroluminescence spectra of Sample 4 at different levels of current injection at room temperature are shown. A picture of the resulting white light and the location of the corresponding operating point on the *(x, y)* coordinates are also displayed. In Figure 5.4.4.2, the evolution of the color rendering index from Sample 1 to Sample 4 is plotted, demonstrating a well-controlled color rendering index tuning and improvement from 49.5 to 83.0 by the controlled layer-by-layer assembly of polyflourene and NCs. Such a high color rendering index satisfies the future lighting requirements of >80 CRI as

road-mapped by Sandia National Laboratories [7], unlike the typical low color rendering index of yellow phosphor coated blue LEDs.

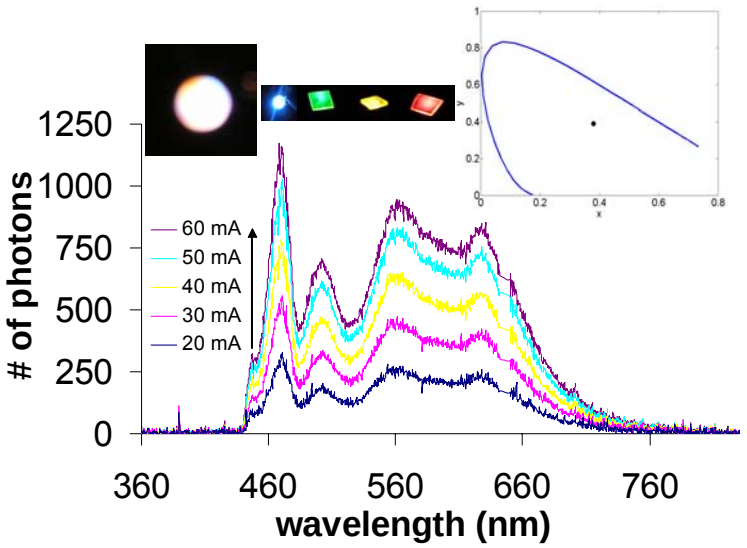

Figure 5.4.4.1. Electroluminescence spectra of blue polyfluorene (λ_{PL} = 439 nm) and yellow, green and red CdSe/ZnS core-shell nanocrystals (λ_{PL} = 580, 540 and 620 nm) layer-by-layer hybridized on a InGaN/GaN n-UV LED (λ_{EL} = 383 nm) at different levels of current injection (room temperature) next to a picture of the generated white light, the blue emitting polymer and green, yellow and red emitting nanocrystals, and the location of the corresponding operating point on the *(x, y)* coordinates.

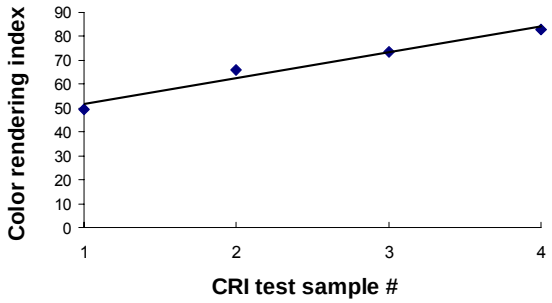

Figure 5.4.4.2. Controlling and improving color rendering index.

5.4.5 White light generation by mixing polyfluoerene and trio combination of nanocrystals

As a control group, alternative to the layer-by-layer integration, the blended mixture of NCs into the polymer is investigated. For that, the mixture contents of the NCs and the polyfluorene are carefully selected to obtain the highest feasible color rendering index while satisfying the white light condition. For that, 20 µl blue polyfluorene (λ_{PL} = 439 nm), 20 µl green NCs (λ_{PL} = 540 nm), 20 µl yellow NCs (λ_{PL} = 580 nm) and 10 µl red NCs (λ_{PL} = 620 nm) with concentrations of 3 mg/ml, 1.3 mg/ml, 1.3 mg/ml and 2.2 mg/ml, respectively, are blended. The n-UV LED (λ_{EL} = 383 nm) is then hybridized with this blend of NCs in the polyfluorene host medium. The electroluminescence spectra of the resulting hybrid device at different levels of current injection at room temperature are given in Figure 5.4.5.1. Additionally, a picture of the generated white light and the location of the corresponding operating point on the *(x, y)* coordinates is displayed in Figure 5.4.5.1. This implementation experimentally leads to *(x, y) = (*0.40*,* 0.38*)*, T_c = 3433 K and R_a = 85.2, again falling within the white region of the C.I.E. chromaticity diagram. In the case of blending, only a single film formation is required and the weighting factors of the contributing photoemission from the emitters in the film are controlled with the emitter concentration, as opposed to the layer-by-layer assembly, which requires multiple emitter film formation and the control of the weighting factors of the emitters with each film thickness. As a result of comparatively easier

hybridization of such NC-polymer blends, a color rendering index that is slightly higher than the layer-by-layer deposition of previous implementation is achieved. However, as also clearly seen in the picture of the generated white light from the NC-polymer blend, strong red emission comes off from the edges of the hybrid device due to the reabsorption at the short wavelengths and significant inhomogeneity of the emitters towards the edges in the blend. Consequently, in our implementation, the approach of layer-by-layer assembly of the NC and polyflourene emitters is observed to be a better choice compared to the blending approach in terms of well-controlled light emission across the entirety of our hybrid device. In Table 5.4.5.1, these hybrid WLEDs presented in this thesis are summarized to list the electroluminescence peak wavelength of the LED, the photoluminescence peak wavelengths of the NCs and polymer emitters, the resulting *(x,y)* tristimulus coordinates, the correlated color temperature T_c, and color rendering index R_a.

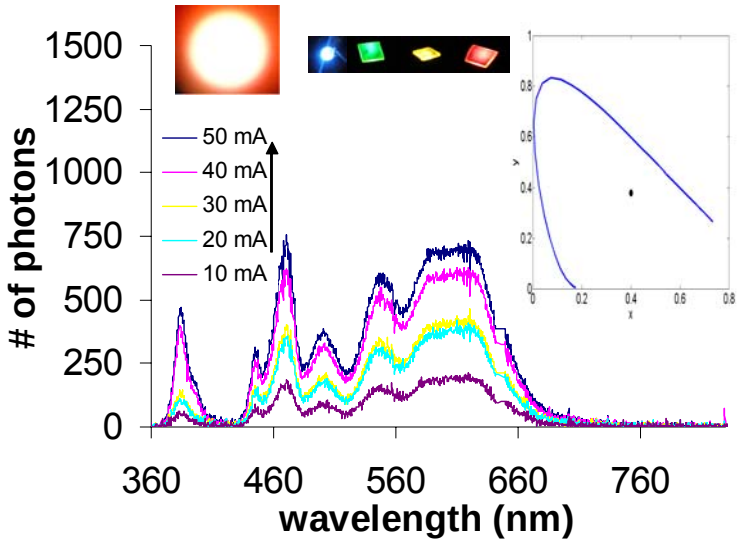

Figure 5.4.5.1. Electroluminescence spectra of blends of blue polyfluorene (λ_{PL} = 439 nm) and yellow, green and red CdSe/ZnS core-shell nanocrystals (λ_{PL} = 580, 540 and 620 nm hybridized on a InGaN/GaN n-UV LED at different levels of current injection at room temperature along with a picture of the generated white light, blue conjugated polymer and green, yellow and red nanocrystals, and the location of the corresponding operating point on the *(x, y)* coordinates.

LED λ_{EL}(nm)	**Polymer** λ_{PL} (nm)	**NC** λ_{PL} (nm)	**(x,y)**	T_c (K)	R_a
383	439	580	(0.31,0.27)	6962	53.4
383	439	540, 580	(0.23,0.30)	14395	65.7
383	439	540, 580, 620	(0.38,0.39)	4052	83.0
383*	439	540, 580, 620	(0.40,0.38)	3433	85.2

Table 5.4.5.1. Hybrid polymer-NC WLED sample characteristics. (The sample with * means that polymer and NCs used as a blended mixture to hybridize the n-UV LEDs.)

Chapter 7

Conclusion

In this thesis, we presented design, growth, fabrication, experimental characterization and theoretical analysis of nanocrystal hybridized light emitting diodes with high color rendering index. We introduced CdSe/ZnS core-shell NCs of the single, dual, trio, and quadruple combinations hybridized with InGaN/GaN LEDs. We adjusted the white light parameters of these hybrid NC-WLEDs such as the tristimulus coordinates, color temperature, and color rending index with the NC type and density and the NC film order and thickness. Afterwards, we showed white light generation with highly tunable optical properties using the hybridization of multiple layer by layer assemblies of CdSe/ZnS core-shell nanocrystals on near ultraviolet (n-UV) InGaN/GaN light emitting diodes. In such UV based hybrid light sources, the hybridized semiconductor nanocrystals are pumped efficiently and virtually all of the visible emission originates from these nanocrystals to contribute collectively to the white light generation. Given the UV technology roadmap, UV LEDs will provide high power excitation platforms to pump the nanocrystals on chip. Moreover, we demonstrated the hybridization of CdSe/ZnS core-shell nanocrystals on InGaN/GaN based blue/near-UV LED to tune color properties (tristimulus coordinates, color correlated temperature, and color rendering

index) of the generated light across the visible and within the white region of the CIE choromacity diagram. Working on 26 samples of hybrid NC-LEDs, we experimentally investigated the effects of NC concentrations and NC film thicknesses on tuning these color properties and discussed layer-by-layer assembly of NCs as opposed to blending in a mixture. Furthermore, the hybridization of our InGaN/GaN n-UV LEDs with different types of CdSe/ZnS core-shell nanocrystals in combination with polyfluorene conjugated polymer were achieved to generate high-quality white light for the first time. With their careful design and device implementation, such hybrid WLEDs were demonstrated to generate white light with high color rendering indices above 80, as is required for future solid state lighting applications.

This thesis work led to submission of 6 science citation index (SCI) journal articles [26,31,34,36,56,57], two of which have been published [26,31] and 12 refereed and invited international conference presentations [27,35,37,58-66]. Our work titled "White light generation using CdSe/ZnS core–shell nanocrystals hybridized with blue InGaN/GaN light emitting diodes" is also highlighted as a featured article on the cover page of the SCI journal Nanotechnology. As final remarks, based on our proof-of-concept demonstrations in this thesis, we believe that such nanocrystal hybridized white light sources hold great promise for future lighting and display applications due to their highly tunable optical properties and high light quality.

BIBLIOGRAPHY

[1] N. Hirosaki, R. Xie, K. Kimoto, T. Sekiguchi, Y. Yamamoto, T. Suehiro, and M. Mitomo, "Characterization and properties of green-emitting b-SiAlON:Eu2+ powder phosphors for white light-emitting diodes," *Appl. Phys. Lett.,* vol. 86, 211905, 2005.

[2] R. Peon, G. Doluweera, I. Platonova, D. Irvine-Halliday, G. Irvine-Halliday, "Solid State Lighting for the Developing World - The Only Solution," *Optics & Photonics 2005, Proceedings of SPIE*, vol. 5941, pp. 109-123, San Diego, 2005

[3] D. Irvine-Halliday, R. Peon, G. Doluweera, I. Platonova, and G. Irvine-Halliday, "Solid State Lighting: The only solution for the developing world," *SPIE Newsroom*, 2006.

[4] Wikipedia, May 2007 <,http://www.wikipedia.com/ledlamp>.

[5] US Department of Energy, "LED application series: Recessed downlights," 2006.

[6] R. V. Steele, "The story of a new light source," *Nature Photonics*, vol. 1, pp. 25-26, 2007.

[7] J. Y. Tsao, "Solid state lighting: Lamps, chips and materials for tomorrow," IEEE Circuits and Devices, vol. 20, pp. 28-37, 2004.

[8] E. F. Schubert, "Light-Emitting Diodes," *Cambridge University Press*, 2006

[9] D. A. B. Miller , Stanford University EE 243 Lecture Notes Stanford, CA, USA: Stanford University, 1997.

[10] M.Yamada, Y. Narukawa, H. Tamaki, Y. Murazaki, and T. Mukai, " A methodological study of the best solution for generating white light," *IEICE Trans. Electron.,* vol. E88–C 9, pp. 1860-1869, 2005.

[11] G. Heliotis, E. Gu, C. Griffin, C. W. Jeon, P. N. Stavrinou, M.D. Dawson and D. D. C. Bradley, "Wavelength-tunable and white-light emission from polymer-converted micropixellated InGaN ultraviolet light-emitting diodes," *J. Opt. A: Pure Appl. Opt.*, vol. 8, pp. 445, 2006.

[12] S. Nakamura, T. Mukai, and M. Senoh, "Candela-class high-brightness InGaN/AlGaN double-heterostructure blue-light-emitting diodes," *Appl. Phys. Lett.*, vol. 64, pp. 1687–1689, 1994.

[13] K. Bando, K. Sakano, Y. Noguchi, and Y. Shimizu, "Development of high-bright and pure-white LED lamps," J. Light Visual Environ., vol.22, no.1, pp.2–5, 1997.

[14] US Department of Energy, "Color quality of white LEDs", 2006.

[15] Evident Technologies, May 2007 <, www.evidenttech.com>.

[16] D. Schoss, A. Mews, A. Eychmüller, and H. Weller, "Quantum-dot quantum well CdS/HgS/CdS: Theory and experiment," Phys. Rev. B, vol. 49, no. 24, 1994.

[17] D. Turnbull, F. Seitz, L. Liebert, "Solid State Physics: Advances in Research and Applications," pp. 234, 1955.

[18] K. Chang, and J. Xia, "Spatially seperated excitons in quantum-dot quantum well structures," *Phys. Rev. B*., vol. 57, no. 16, 1998.

[19] D. Battaglia, B. Blackman, and X. Peng, "Coupled and Decoupled Dual Quantum Systems in One Semiconductor Nanocrystal," *J. Am. Chem. Soc*., vol. 127, no. 31, 2005.

[20] S. Sapra and D. D. Sarma, "Evolution of the electronic structure with size in II-VI semiconductor nanocrystals," *Phys. Rev. B***,** vol. 69, 2004.

[21] B. O. Dabbousi, J. Rodriguez-Viejo, F. V. Mikulec, J. R. Heine, H. Mattoussi, R. Ober, K. F. Jensen, , and M. G. Bawendi, "(CdSe)ZnS Core-Shell Quantum Dots: Synthesis and Characterization of a Size Series of Highly Luminescent Nanocrystallites," *J. Phys. Chem. B*, pp. 9463-9475 1997.

[22] S. Nakamura and G. Fasol, "The Blue Laser Diode", (Berlin: Springer)

[23] H. Chen, D. Yeh, C. Lu, C. Huang, W. Shiao, J. Huang, C. C. Yang, I. Liu, and W. Su," White Light GenerationWith CdSe–ZnS Nanocrystals Coated on an InGaN–GaN Quantum-Well Blue/Green Two-Wavelength Light-Emitting Diode," *IEEE Photon. Technol. Lett.*,vol. 18, pp. 1430-1432, 2006.

[24] H. Chen, C. Hsu, and H. Hong, "InGaN–CdSe–ZnSe Quantum Dots White LEDs," *IEEE Photon. Technol. Lett.*, vol. 18, pp. 193-195, 2006.

[25] M. A. Petruska, D. D. Koleske, M. H.Crawford, and V. I. Klimov, "Nanocrystal-Based Light-Emitting Diodes Utilizing High-Efficiency

Nonradiative Energy Transfer for Color Conversion," *Nanoletters*, vol. **6,** pp.1396-1400, 2006.

[26] S. Nizamoglu, T. Ozel, E. Sari and H. V. Demir, "White light generation using CdSe/ZnS core-shell nanocrystals hybridized with InGaN/GaN light emitting diodes," *Nanotechnology*, vol. 18, 2007.

[27] S. Nizamoglu, T. Ozel, E. Sari, and H. V. Demir, "White light generation with CdSe/ZnS core-shell nanocrystals and InGaN/GaN light emitting diodes," IEEE COMMAD Conference on Optoelectronic and Microelectronic Materials and Devices (Perth, Australia) WO-A5.

[28] A. Sandhu, "The future of ultraviolet LEDs," *Nature Photon.,* vol 1**,** pp.38, 2007.

[29] D. V. Talapin, A. L. Rogach, A. Kornowski, M. Haase, and H. Weller, "Highly Luminescent Monodisperse CdSe and CdSe/ZnS Nanocrystals Synthesized in a Hexadecylamine-Trioctylphosphine Oxide-Trioctylphospine Mixture," *Nano Lett.,* vol. 1, pp. 207-211, 2007.

[30] E. Mutlugun, I. M. Soganci, and H. V. Demir, "Nanocrystal hybridized scintillators for enhanced detection and imaging on Si platforms in UV," *Optics Express*, vol. 15, pp.1129 2007.

[31] E. Sari, S. Nizamoglu, T. Ozel, and H. V. Demir, "Blue quantum electroabsorption modulators based on reversed quantum confined Stark effect with blue shift," *Appl. Phys. Lett.* ,vol. 90, no. 011101, 2007

[32] V. A. Sabnis, H. V. Demir, O. Fidaner, J. S. Harris, D. A. B. Miller, J. F. Zheng, N. Li, T. C. Wu, H. T. Chen, and Y. M. Houng, "Intimate Monolithic integration of Chip-scale Photonic Circuits," *Appl. Phys. Lett.*, vol. 84 , pp. 469-471, 2004.

[33] H. V. Demir, V. A. Sabnis, J. F. Zheng, O. Fidaner, J. S. Harris, and D. A. B. Miller, "Scalable wavelength-converting crossbar switches," *IEEE Photon. Technol. Lett.*, vol. 16, pp. 2305-2307, 2004.

[34] S. Nizamoglu and H. V. Demir, "Nanocrystal based white light generation with tunable color parameters by using blue and n-UV InGaN/GaN light emitting diodes", *J. Opt. A: Pure Appl. Opt.,* 2007 (Accepted).

[35] S. Nizamoglu, and H. V. Demir, "Nanocrystal hybridized white light sources integrated on near UV LEDs," to appear in the Proceedings of *International Conference on Physics, Chemistry, and Applications of Nanostructures (Nanomeeting-2007)*, Minsk, Belarus (22-25 May 2007).

[36] S. Nizamoglu and H. V. Demir, "Hybrid white light sources based on layer by layer assembly of nanocrystals on n-UV emitting diodes", 2007 (Submitted).

[37] S. Nizamoglu, T. Ozel, E. Sari, and H. V. Demir, "Tunable White Light Generation," *2007 Nanometa Conference*, Seefeld, Austria (8-11 January 2007).

[38] K. L. Paik, N. S. Baek, H. K. Kim, J-H. Lee, and Y. Lee, "White Light-Emitting Diodes from Novel Silicon-Based Copolymers Containing Both Electron-Transport Oxadiazole and Hole-Transport Carbazole Moieties in the Main Chain," *Macromolecules*, vol. **35**, pp. 6782, 2002.

[39] K. E. Cheon and J. Shinar, "Bright white small molecular organic light-emitting devices based on a red-emitting guest–host layer and blue-emitting 4,4‴-bis(2,2′-diphenylvinyl)-1,1′-biphenyl," *Appl. Phys. Lett.,* vol. 81, pp. 1738, 2002.

[40] C. H. Chuen and Y. T. Tao, "Highly-bright white organic light-emitting diodes based on a single emission layer," *Appl. Phys. Lett.*, vol. 81, pp. 4499, 2002.

[41] B. D'Andrade, "White phosphorescent LEDs offer efficient answer," *Nature Photonics*, vol. 1, pp. 33, 2007.

[42] J. Kido, M. Kimura, and K. Nagai, "Multilayer White Light-Emitting Organic Electroluminescent Device," *Science,* vol. 267, pp. 1332, 1995.

[43] G. Cheng, F. Li, Y. Duan, J. Feng, S. Liu, S. Qiu, D. Lin, Y. Ma, and S. T. Lee, "White organic light-emitting devices using a phosphorescent sensitizer," *Appl. Phys. Lett* ,vol. 82, pp. 4224, 2003.

[44] R. H. Jordan, A. Dodabalapur, M. Strukelj, and T. M. Miller, "White organic electroluminescence devices," *Appl. Phys. Lett*., vol. 68, pp. 1192, 1996.

[45] B. W. D'Andrade, M. E. Thompson, and S. R. Forrest, "Controlling Exciton Diffusion in Multilayer White Phosphorescent Organic Light Emitting Devices," *Adv. Mater.*, vol. 14, pp. 147, 2002.

[46] B. W. D'Andrade, J. Brooks, V. Adamovich, M. E. Thompson, and S. R. Forrest, *Ann. Telecommun. ,* vol. 14, pp.1032, 2002.

[47] S-A. Chen, K-R. Chuang, C-I. Chao, and H-T. Lee, *Synth. Met.,* vol. 82, pp. 207, 1996.

[48] M. Granström and O. Inganäs, "White light emission from a polymer blend light emitting diode," *Appl. Phys. Lett.,* vol. 68, pp. 147, 1996.

[49] S. Tasch, E. J. W. List, O. Ekström, W. Graupner, G. Leising, P. Schlichting, U. Rohr, Y. Geerts, U. Scherf, and K. Müllen, " Efficient white

light-emitting diodes realized with new processable blends of conjugated polymers," *Appl. Phys. Lett.*, vol. 71, pp. 2883, 1997.

[50] F. Steuber, J. Staudigel, M. Stössel, J. Simmerer, A. Winnacker, H. Spreitzer, F. Weissörtel, and J. Salbecki, " White Light Emission from Organic LEDs Utilizing Spiro Compounds with High-Temperature Stability," *Adv. Mater.,* vol. 12, pp. 130, 2000.

[51] Y-Z. Lee, X. Chen, M-C. Chen, and S-A. Chen, "White-light electroluminescence from soluble oxadiazole-containing phenylene vinylene ether-linkage copolymer," *Appl. Phys. Lett.,* vol. 79, pp. 308, 2001.

[52] R. S. Deshpande, V. Bulovic, and S. R. Forrest, "White-light-emitting organic electroluminescent devices based on interlayer sequential energy transfer," *Appl. Phys. Lett.,* vol. 75, pp. 888, 1999.

[53] M. Strukelj, R. H. Jordan, and A. Dodabalapur, "Organic multilayer light emitting diodes," *J. Am. Chem. Soc.*, vol. 118, pp. 1213, 1996.

[54] E. J. W. List, G. Leising, N. Schulte, D. A. Schluer, U. Scherf, W. Graupner, *Jap. J. Appl. Phys. Part 2: Lett,* ,vol. 39 ,pp. L760, 2000.

[55] D. Neher, *"*Polyfluorene Homopolymers: Conjugated Liquid-Crystalline Polymers for Bright Blue Emission and Polarized Electroluminescence,*" Macromol. Rapid Commun.,* vol. 22, pp. 1365, 2001.

[56] I. O. Huyal, T. Ozel, U. Koldemir, S. Nizamoglu, D. Tuncel, and H. V Demir, "White light emission with high color rendering index >90 from single-layer azide functionalized polyfluorene-copolymer on near-UV light emitting diode," 2007 (In submission).

[57] H. V. Demir, S. Nizamoglu, T. Ozel, E. Mutlugun, I. O. Huyal, E. Sari, E. Holder and N. Tian, "White light generation tuned by dual hybridization of nanocrystals and conjugated polymers," 2007 (Submitted).

[58] H. V. Demir, E. Mutlugun, S. Tek, S. Nizamoglu, I. M. Soganci, E. Sari, T. Ozel, I. O. Huyal, G. Zengin, and C. Uran, "Functional Nanophotonic Materials for Hybrid Use in Optoelectronics," *The 2007 Material Science and Technology Conference and Exhibition, Nanostructured Ceramic Materials, Science and Technology Symposium: Functional Behavior and Characterization of Nanomaterials*, Detroit, Michigan (16-20 September 2007). Invited Paper.

[59] H. V. Demir, S. Nizamoglu, E. Mutlugun, T. Ozel, I. M. Soganci, S. Tek, I. O. Huyal, E. Sari, G. Zengin, and C. Uran, "Hybrid Nanophotonic Approaches for New Functionality," to appear in the Proceedings of *SPIE Optics East*

Conference on Optoelectronic Devices: Physics, Fabrication, and Application), Boston, MI (9-12 September 2007). Invited Paper.

[60] T. Ozel, E. Sari, S. Nizamoglu, and H. V. Demir, "Near-UV InGaN/GaN-based Quantum Optoelectronic Devices," to appear in the Proceedings of *SPIE Europe Microtechnologies for the New Millennium*, Maspalomas, Gran Canaria, Spain (2-4 May 2007).

[61] E. Sari, S. Nizamoglu, T. Ozel, and H. V. Demir, "Blue InGaN/GaN-based Quantum Electroabsorption Modulators," Proceedings of *IEEE Conference on Optoelectronic and Microelectronic Materials and Devices (COMMAD 2006)*, Perth, Australia (6-7 December 2006). Paper WO-A4.

[62] E. Sari, S. Nizamoglu, T. Ozel, H. V. Demir, A. Inal, E. Ulker, E. Ozbay, Y. Dikme and M. Heuken, "InGaN/GaN based LEDs with electroluminescence in violet, blue, and green tuned by epitaxial growth temperature," Proceedings of *IEEE Lasers and Electro-Optics Society 2006 Annual Meeting (LEOS 2006)*, Montreal, QC, Canada (29 October – 2 November 2006). Paper MC3.

[63] E. Mutlugun, I. M. Soganci, E. Sari, T. Ozel, S. Nizamoglu, and H. V. Demir, "Hybrid nanophotonic devices: UV scintillators and visible/UV modulators," Proceedings of *the 50th IUVSTA Meeting Toward novel nanostructure-based devices:nanostructured materials fabrications, characterization and assembly for novel devices*, Dubrovnik, Croatia (22-27 October 2006).

[64]H. V. Demir, E. Sari, T. Ozel, and S. Nizamoglu, "Optical quantum modulators for UV communication in space," Proceedings of *European Optical Society Annual Meeting (EOS 2006)*, Paris, France (16-19 October 2006).

[65] H. V. Demir, E. Sari, E. Mutlugun, I. M. Soganci, T. Ozel, and S. Nizamoglu, "Photonic functions in UV enabled by in-solution synthesized nanocrystals and epitaxially grown quantum structures," *NanoTX*, Dallas, TX (27-28 September 2006). Invited paper.

[66] I. O. Huyal, T. Ozel, S. Nizamoglu, U. Koldemir, D.Tuncel, and H. V. Demir, "White Light Generation with Azide Functionalized Polyfluorene Hybridized on Near-UV Light Emitting Diode," to appear in the Proceedings of *the Conference on Lasers and Electro-Optics (CLEO 2007) and the Quantum Electronics and Laser Science Conference (QELS 2007)*, Baltimore, Maryland, USA (6-11 May 2007).